AD-A031 586 WOODS HOLE OCEANOGRAPHIC INSTITUTION MASS F/G 8/11
REFLECTION ENERGETICS AND ACOUSTIC IMPEDANCE OF THE SEABED FROM--ETC(U)
SEP 76 S T KNOTT, H HOSKINS, E O LACASCE N00014-74-C-0262
UNCLASSIFIED WHOI-76-88 NL

END
DATE FILMED
12-76

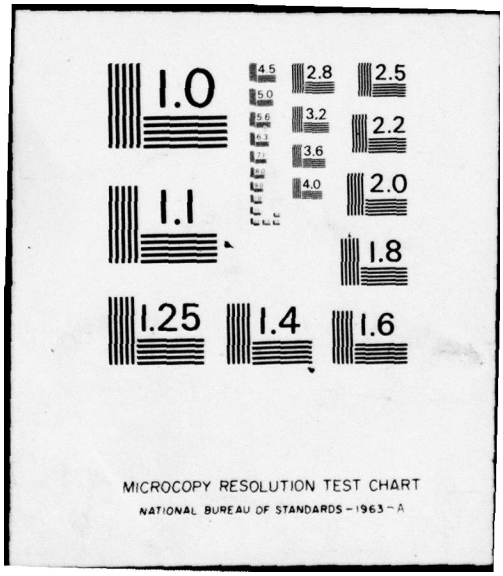
1.0
1.1
1.25
1.4
1.6
1.8
2.0
2.2
2.5
2.8
3.2
3.6
4.0
4.5
5.0
5.6
MICROCOPY RESOLUTION TEST CHART
NATIONAL BUREAU OF STANDARDS - 1963 - A

UNCLASSIFIED 9/76

SECURITY CLASSIFICATION OF THIS PAGE (When Data Entered)

REPORT DOCUMENTATION PAGE

READ INSTRUCTIONS BEFORE COMPLETING FORM

1. REPORT NUMBER: WHOI-76-88	2. GOVT ACCESSION NO: —
3. RECIPIENT'S CATALOG NUMBER: (9)	
4. TITLE (and Subtitle): (6) REFLECTION ENERGETICS AND ACOUSTIC IMPEDANCE OF THE SEABED FROM NORMAL-INCIDENCE SEISMIC REFLECTIONS - SOMALI BASIN.	5. TYPE OF REPORT & PERIOD COVERED: Technical rept.
	6. PERFORMING ORG. REPORT NUMBER:
7. AUTHOR(s): (10) S. T. Knott, Hartley Hoskins and E. O. LaCasce, Jr.	8. CONTRACT OR GRANT NUMBER(s): (15) N00014-74-C-0262; NSF-GA-27516
9. PERFORMING ORGANIZATION NAME AND ADDRESS: Woods Hole Oceanographic Institution, Woods Hole, MA 02543	10. PROGRAM ELEMENT, PROJECT, TASK AREA & WORK UNIT NUMBERS: NR 083-004
11. CONTROLLING OFFICE NAME AND ADDRESS: Office of Naval Research, Code 480	12. REPORT DATE: (11) September 1976
	13. NUMBER OF PAGES: 71
14. MONITORING AGENCY NAME & ADDRESS (if different from Controlling Office): (12) 77p.	15. SECURITY CLASS. (of this report): Unclassified
	15a. DECLASSIFICATION/DOWNGRADING SCHEDULE

16. DISTRIBUTION STATEMENT (of this Report)

Approved for public release; distribution unlimited.

17. DISTRIBUTION STATEMENT (of the abstract entered in Block 20, if different from Report)

18. SUPPLEMENTARY NOTES

19. KEY WORDS (Continue on reverse side if necessary and identify by block number)

1. Seismic reflection profiling
2. Reflection energetics of seismic profiling
3. Acoustic impedance estimates from seismic reflections

20. ABSTRACT (Continue on reverse side if necessary and identify by block number)

Useful estimates of seabed acoustic impedance variations in depth and location can be derived from measurements of the travel time rate at which low frequency normal incidence reflected seismic energy is received. Analysis techniques are straightforward and easily applied to station data and to traverse profiles to evaluate the lateral continuity of material properties from one location to another. Added to critical judgment, geological and geophysical evidence, e.g. drill-hole cores, outcrops and interval and critical refraction velocity measurements, reflection energetics measurements provide →

next page AB

DD FORM 1 JAN 73 1473 EDITION OF 1 NOV 65 IS OBSOLETE S/N 0102-014-6601

UNCLASSIFIED 9/76

SECURITY CLASSIFICATION OF THIS PAGE (When Data Entered)

381 000

improved insight with which to justify classifications of seabed materials within the constraints of available information.

The analysis technique is tested using reflection data from six stations and two profiles in the environs of the Somali Basin. Two clearly different impedance-depth distributions are evident, one to the northwest of Chain Ridge is near-linear down through the sediments and including basement, the other to the south of the basin proper exhibits a near-uniform low impedance throughout the sediment column with sharp increases at or near basement, in agreement with that found nearby at Deep Sea Drilling Project site #235. Continuity of material properties is more uniform in the southern data than the northern where local variations in seafloor reflectivity and seabed response are evident.

Major conclusions from our "audit" of reflected energy are that reflection energetics measurements and impedance estimates agree with and/or corroborate the other geological and geophysical evidence, and that such an audit has unique utility in the interpretation of seismic reflection profiles, particularly as to the degree of lateral continuity in the seabed physical properties. Logical extension of the technique to higher frequencies will provide higher resolution for assessing the surficial seabed characteristics.

WHOI-76-88

REFLECTION ENERGETICS AND ACOUSTIC IMPEDANCE OF THE SEABED FROM NORMAL-INCIDENCE SEISMIC REFLECTIONS - SOMALI BASIN

by

S. T. Knott, Hartley Hoskins and
E. O. LaCasce, Jr.

WOODS HOLE OCEANOGRAPHIC INSTITUTION
Woods Hole, Massachusetts 02543

September 1976

TECHNICAL REPORT

Prepared for the Office of Naval Research under Contract N00014-74-C-0262; NR 083-004 and for the National Science Foundation under Grant GA-27516.

Approved for public release; distribution unlimited.

Approved for Distribution John I. Ewing

John I. Ewing, Chairman
Department of Geology & Geophysics

ABSTRACT

Useful estimates of seabed acoustic impedance variations in depth and location can be derived from measurements of the travel time rate at which low frequency normal incidence reflected seismic energy is received. Analysis techniques are straightforward and easily applied to station data and to traverse profiles to evaluate the lateral continuity of material properties from one location to another. Added to critical judgment, geological and geophysical evidence, e.g. drill-hole cores, outcrops and interval and critical refraction velocity measurements, reflection energetics measurements provide improved insight with which to justify classifications of seabed materials within the constraints of available information. Methods to map seabed response characteristics are discussed.

The analysis technique is tested using reflection data from six stations and two profiles in the environs of the Somali Basin. Two clearly different impedance-depth distributions are evident, one to the northwest of Chain Ridge is near-linear down through the sediments and including basement, the other to the south of the basin proper exhibits a near-uniform low impedance throughout the sediment column with sharp increases at or near basement, in agreement with that found nearby at Deep Sea Drilling Project site #235. Continuity of material properties is more uniform in the southern data than the northern where local variations in seafloor reflectivity and seabed response are evident.

Major conclusions from our "audit" of reflected energy are that reflection energetics measurements and impedance estimates agree with and/or corroborate the other geological and geophysical evidence, and that such an audit has unique utility in the interpretation of seismic reflection profiles, particularly as to the degree of lateral continuity in the seabed physical properties. Logical extension of the technique to higher frequencies will provide higher resolution for assessing the more surficial seabed characteristics.

TABLE OF CONTENTS

TABLE OF CONTENTS (Continued)

INTRODUCTION

When we attempt to interpret continuous seismic reflection profiles it is not easy to ignore the desire and need to classify in some way the differences in physical properties of the sediment and rock that cause the reflection horizons that are observed. Much of such classification is based upon critical judgment. A significant part is based upon determinations of the interval and critical-refraction velocities of the sediments and rock derived from wide-angle reflection-refraction profiles obtained with sonobuoys (LePichon et al., 1968), upon sampled outcrops, and upon the cores retrieved and the down hole measurements made at drill-hole sites, particularly those of the Deep Sea Drilling Program (DSDP).

Sonobuoys and drill-holes are site-or station-type observations so it becomes a question as to how far one can extrapolate the classifications at such sites to other locations primarily on the basis of the continuity of reflection horizons. Even if good continuity is observed there are often large apparent changes in reflected energy that cause one to wonder how constant or variable the contrast in materials may be along a given horizon traced from one location to another.

In this paper we describe how we have evolved and used a relatively straight-forward method for systematically deriving estimates of the acoustic impedance of the seabed materials and the impedance variation with depth and location using low frequency normal-incidence reflections. ("Seabed"is used to imply everything below the sea floor.) We have sought such estimates not only to improve our ability to extrapolate classifications between sampling sites, but also these measurements like those of velocity provide an added dimension which must be justified within the context of the physical and geological interpretations of the reflection profiles. It is readily understood that knowledge of velocity-depth variations is essential to the determination of sediment thicknesses, to the quantitative assessment of sediment volume and to geologic inferences that relate velocity to type of material, age and consolidation. Estimates of acoustic impedance complement, corroborate or deny, the same suite of critical judgments and classifications giving better definition to our inferences.

To demonstrate the use of this method we have examined seismic reflection energetics at six locations (sonobuoy stations #3, #4, #8, #14, #15 and #17) in or near the environs of the Somali Basin (Fig. 1). We chose to make this study of the Somali because the wide extent of somewhat similar sedimentary structure of varying thicknesses above oceanic basement permits relatively simple comparisons of reflection energetics, and because cores from DSDP #235, near station #14, cover most of the sedimentary structure down to basement (Fisher, Bunce et al. 1974). Wide-angle and normal incidence profile data, tape recorded at each sonobuoy station, are used in the analyses, wide-angle for velocity structure, and normal incidence for reflectivity measurements from which impedance estimates are derived, and from which the continuity of the contrasts in seabed materials is evaluated.

BACKGROUND

Mapping the distribution, thickness and structure of the sedimentary accumulations and underlying crustal structures below the seafloor are important scientific objectives. The principle techniques involved, normal-incidence and wide-angle reflection profiling and refraction profiling, are each based primarily upon acoustic travel time measurements. The propagation velocities determined by the latter two techniques are used with the first to determine structure thicknesses and shapes, and to characterize the materials involved by their propagation velocities.

Of the three techniques, normal-incidence profiling has been the most extensively employed, probably because it produces a readily assayable graphic record. The shot-to-shot continuity and coherence in travel time of the reflection wavelets along a profile has made possible the delineation of the reflection horizons that are inferred to be representative of geological structure occurring beneath the ocean floor.

Thus, there has evolved a sizable literature on the interpretation and classification of the observed reflection horizons, on speculations as to the causes of the observed structures, and the correlation of the reflection horizons to particular geological structures revealed by coring and deep sea drilling. The effectiveness of the seismic reflection technique was demonstrated (Hersey & Ewing, 1949; Officer, 1955; Shor, 1959; Hersey, 1963; Ewing, J., 1963), applied to regional studies (e.g. Ewing, J., et al, 1962;

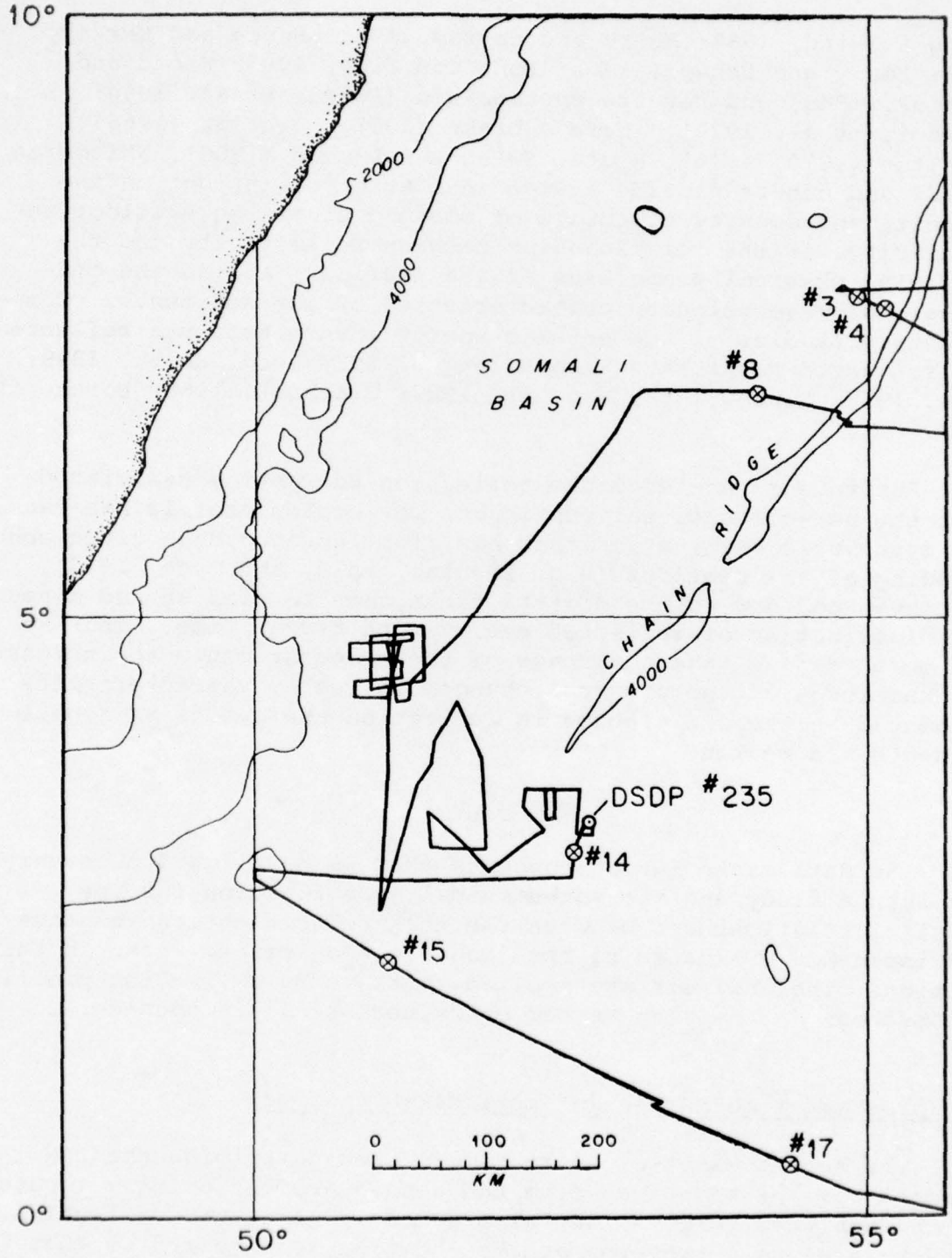

FIG. 1 Ship's track of R/V CHAIN cruise 100-4 with locations of the six seismic reflection stations and DSDP site #235, Somali Basin and environs.

Ewing & Ewing, 1962; Moore and Curray, 1963; Bunce and Hersey, 1966; Emery and Uchupi, 1965; Rona and Clay, 1967; Knott and Hoskins, 1968) and results synthesized (Ewing, et al, 1964; Talwani, et al, 1972). Nafe & Drake (1957), Breslau (1966), Hamilton (1970,71,76), Houtz, Ewing & LePichon (1968), Whitmarsh (1972) and others provide a wide foundation of insight on the velocity and density structure of oceanic crust, on seafloor reflectivity, on the relationships between reflectivity and the surficial physical properties of the seafloor, and on the compressional wave velocity characteristics of the sediments. Complementary studies of the seismic energy transmitted via reflected and refracted paths have also a long history (e.g. Knott, 1899; Nafe, 1957; Gupta, 1965, Hermont, 1967; Claebout, 1968; Borcherdt, 1973.

But to our knowledge the reflection energetics associated with the now-conventional continuous reflection profile has lacked the systematic examination that has, for instance,been given echo sounding of the seafloor (e.g. Breslau, ibid, and Tyce, 1976). It is convenient now to use digital techniques to display and measure the distribution of reflected energy with travel time. Thus we can more readily take advantage of these measurements to increase our knowledge of the physical changes in seabed characteristics evidenced in the differences in reflection energetics as functions of depth and region.

TECHNIQUE

The data manipulation concepts that we have found necessary for such a study and the mathematical justification for the physical relationships between the measured reflection response and impedance estimates of the seabed are described first in this section. The analyses are applied to traverse reflection profiles, and methods for mapping seabed characteristics are considered.

The pressure-time curves and reflection profiles

The shot-by-shot pressure time curves comprising the reflected wavelet sequences from the seabed are the primary inputs to the analyses (Fig. 2),but also a knowledge of the reflection structure along a traverse at the location is required so that phenomena such as side echoes and basement relief can be identified

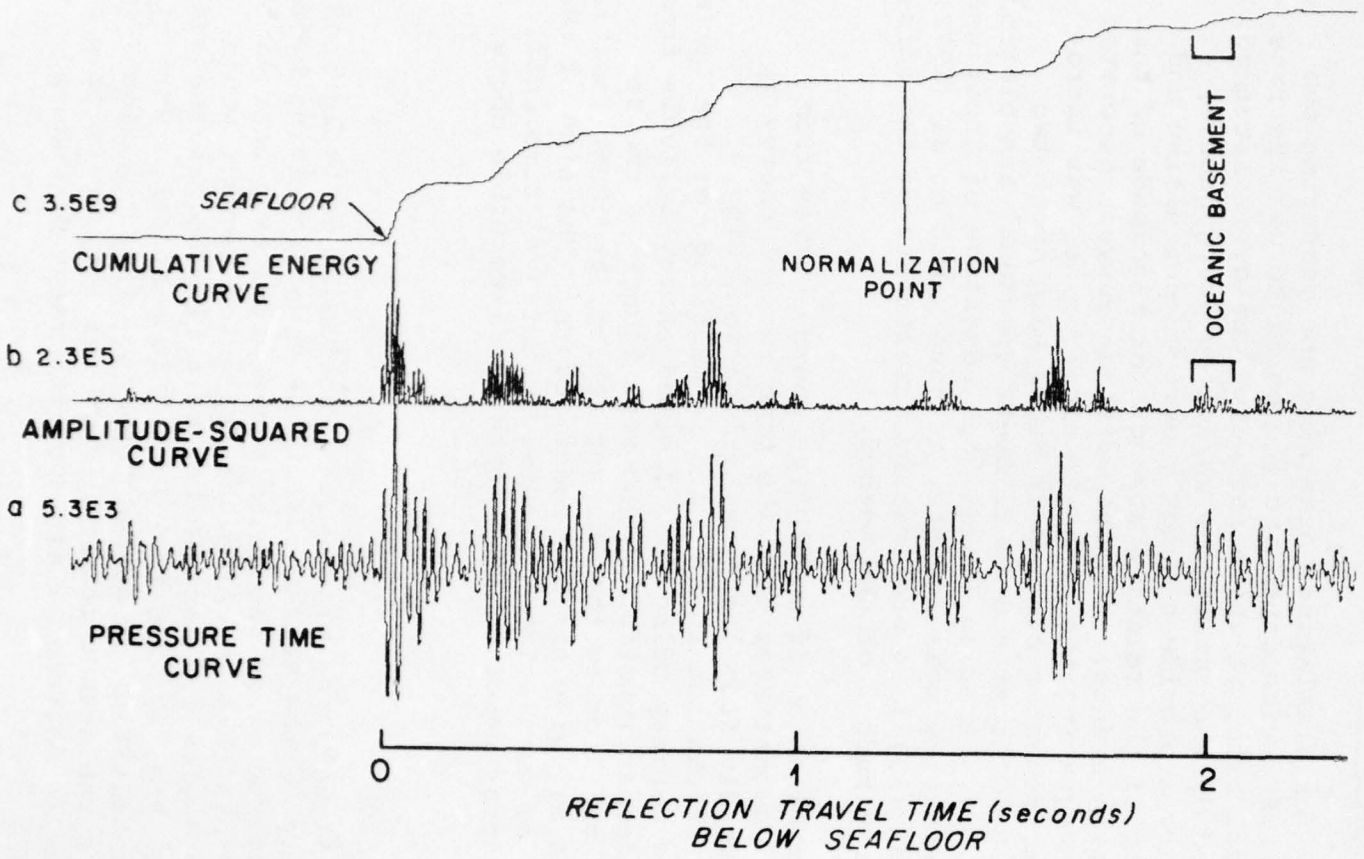

FIG. 2 The reflection sequence displayed in three forms: the pressure-time curve, an amplitude-squared curve, and the cumulative energy curve. The maximum values of the amplitude and amplitude-squared traces are normalized to a standard unit deflection. Values "a" and "c" are the values of the amplitude and cumulative energy traces at their respective normalization points, and "b" the per point average background noise energy determined in a time window before the onset of the seafloor reflection.

and avoided if possible (Fig. 3).

The Cumulative Energy Curve

Our strategy for displaying, examining and measuring the changes in reflectivity with depth and region is to use the rate, in respect to travel time, at which reflected energy is returned. This is represented by the cumulative reflected energy curve, Figure 2. Such curves provide a quickly derived definitive and accurate assessment of the relative strength or magnitude of the successive reflection events. The use of these curves, generated by squaring and integrating the pressure time curves, was introduced in underwater acoustic studies at Woods Hole about two decades ago by C. B. Officer and F. T. Dietz (personal association) and Baxter (1958, 60). Breslau (ibid) took advantage of their use for seafloor reflectivity measurements, as have Knott et al (1972) and Baggeroer et al (1973) in preliminary assessments of the seismic reflected energy budget of the seabed.

A cursory examination of cumulative energy curves from various locations demonstrates that the time rate of energy reception varies markedly from location to location, Fig. 4. Of interest is the distribution in time and in magnitude of the series of steps and ramps corresponding to reflected energy arrivals from the seafloor and deeper interfaces. At some locations the reflection from the seafloor is the largest return, at other locations a deeper interface may give the strongest return. The size of the steps or the rate of cumulation decreases with travel time until finally no more energy received from depth is discernible above noise.

Noise

Reflection signals are mixed with a continuum of background noise due primarily to the self-noise of the towed receiving hydrophone array. Integration of the noise alone produces a near linear ramp. To remove this ramp on which the reflected signals would appear, the noise energy is measured per unit time before the seafloor return (b in Fig. 2), and this amount is subtracted per unit time during the integration of seabed returns. Thus the signal-to-noise ratio during the seabed returns is in rea lity unity or 0 dB whenever the trace is horizontal although the ratio may exceed

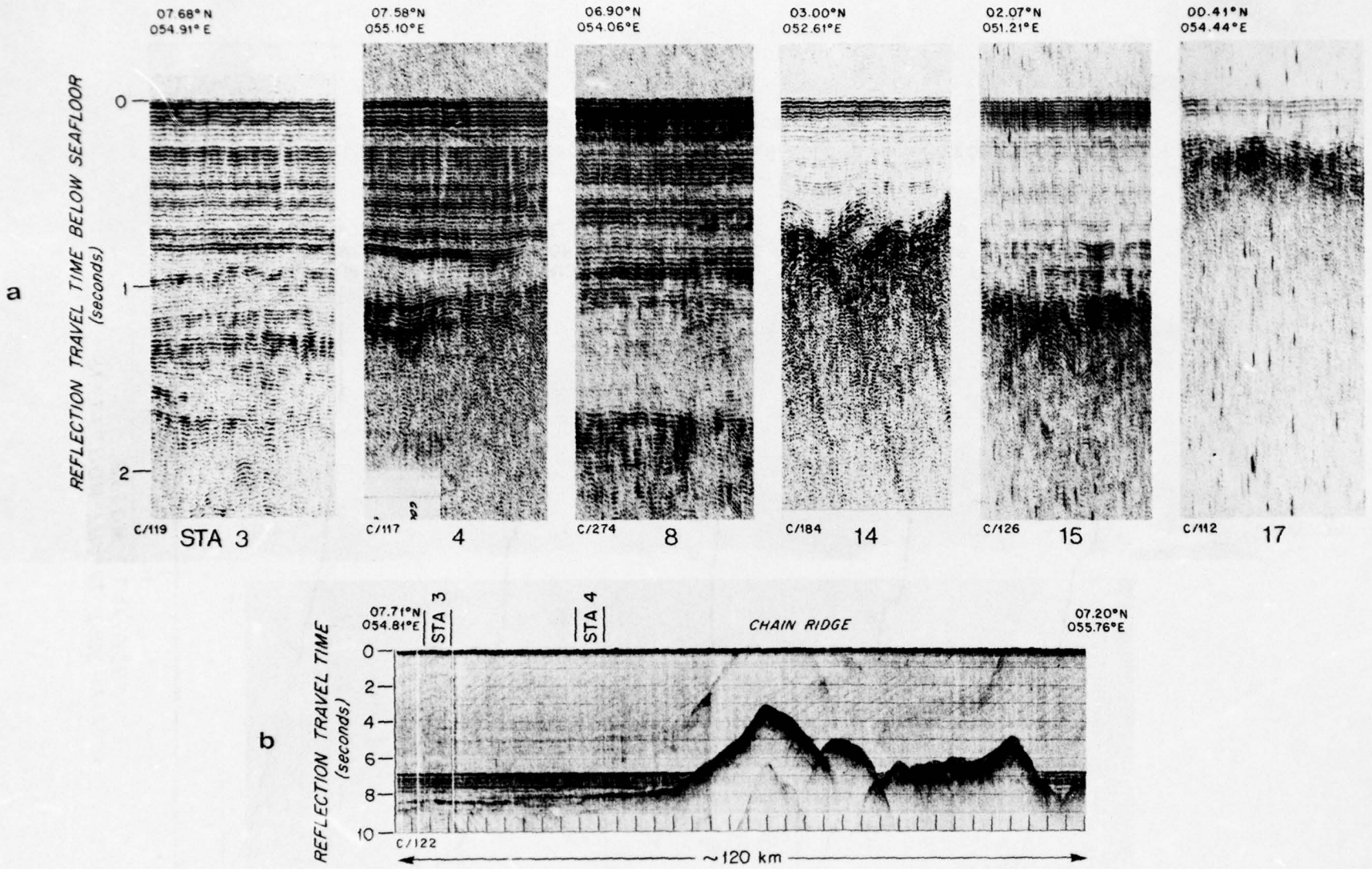

FIG. 3 (a) Reflection profiler recordings at the six stations.

(b) Profiler recording showing continuity in sediment reflections between stations #3 and #4, adjacent to Chain Ridge basement outcrops.

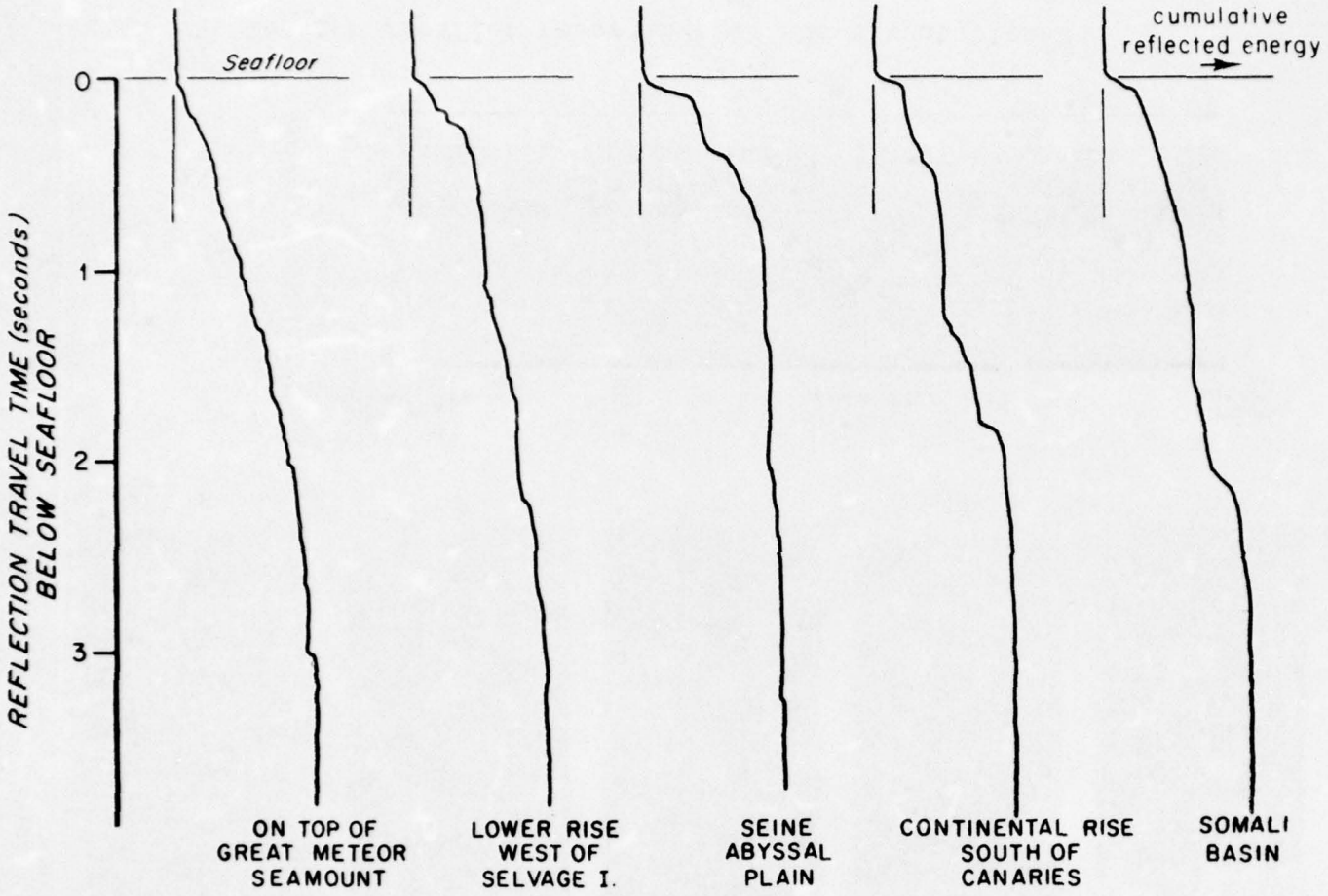

FIG. 4 Cumulative energy traces from several sites. (Maximum deflection normalized to a standard unit deflection).

20 dB for the sea floor reflection. Obviously the lower the noise the better the determinations.

Normalization of trace

Note that the cumulative energy curves (integrands, for brevity) that are displayed for simple comparison in Figure 4 are normalized to a common terminal deflection, whereas in Figure 2 the normalization point of the integrand is mid-trace and the magnitude (relative to the quiescent trace) of cumulative energy at that point is given (c in Fig. 2).

In general, normalization provides a means to control the size of recordings, and combined with measurements of the amplitude or energy at the normalization point (norm point) it establishes scale. Most important to this study, normalization relative to a common basis permits comparisons of the relative rates of change in magnitude of the cumulative reflected energy from one shot to that of another in a situation in which the actual energy of each shot is unknown. Within a given bandwidth the relative energetic response of the seabed at a given location can be expected to be reasonably repeatable from shot to shot even if the absolute shot-to-shot energy levels are unknown but within practical limits. Thus similar shaped integrands are expected from shot to shot provided the curves are similarly normalized (Fig. 5). The selected position of the norm point in travel time establishes a unit reference deflection representing the energy cumulated from the onset of the seafloor returns to the reception of some particular reference reflection horizon, such as, oceanic basement, an intermediate sediment horizon, the sea floor, or between horizons at a quiescent point in the traces. Like most acoustic data, shot-to-shot variations are expected in the energy cumulated up to the norm point. These variations tend to become greater with increasing travel time because of the cumulative effect of early variations upon those arrivals that occur later, and because the roughness of reflection horizons commonly increases with depth. Thus the integrand that typifies the response at a given location is derived by smoothing the data.

Two methods were examined for deriving a representative average-shape integrand, 1) an average of similarly normalized integrands, 2) the integrand of the average of several pressure-

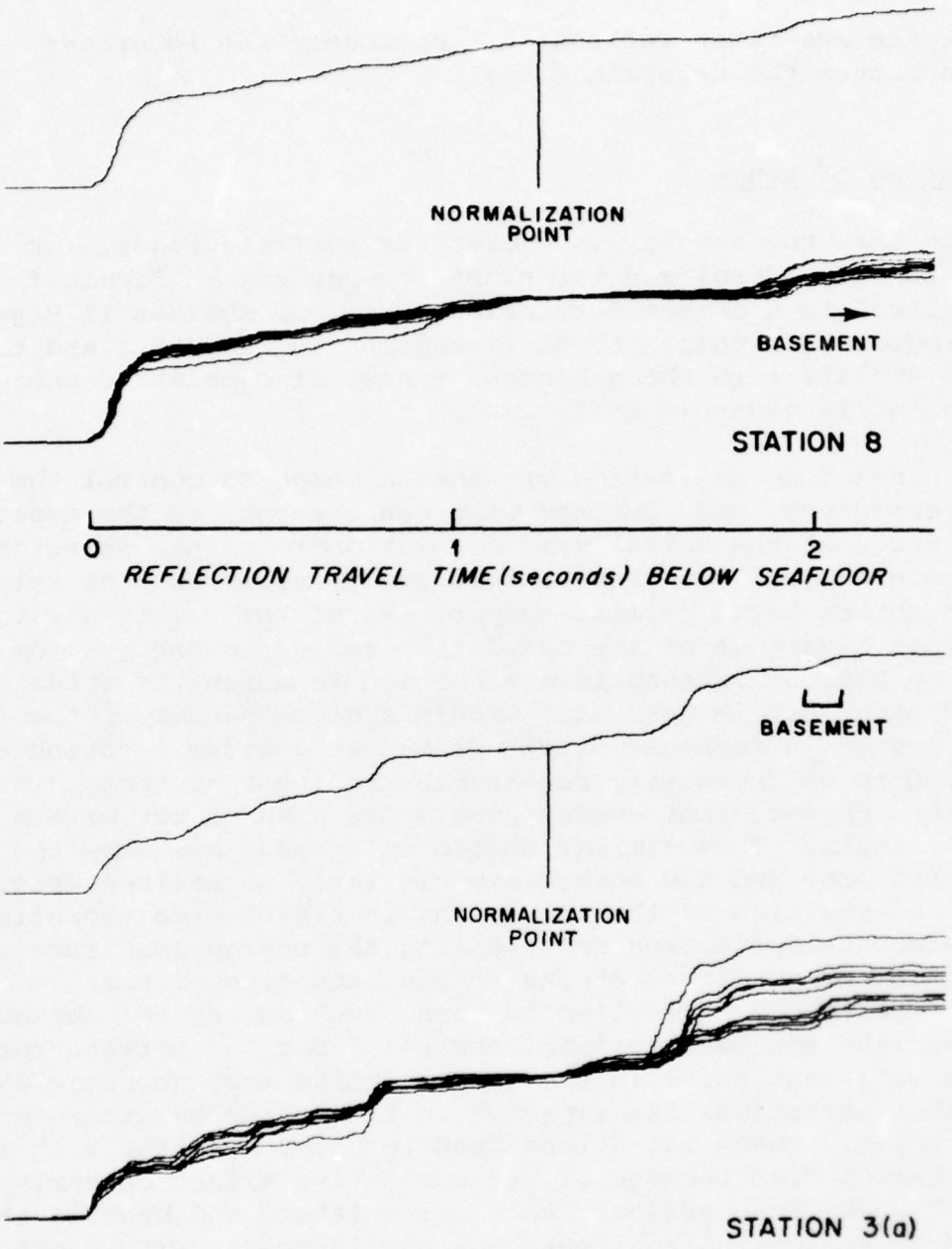

FIG. 5 Graphic comparison of the response of ten shots (stations #3a and #8) from which an average-shape integrand is computed. The traces are aligned in travel time on the seafloor reflection and have a common deflection at the norm point. The average-shape integrand is the representative cumulative energy curve for each station. Data for station #3 was taken from the beginning of profile (Fig. 3).

time curves. The first option produces the better representation for the data at hand and is used in this study, Figure 5. Although an average of amplitude traces improves the signal-to-noise ratio for coherent signals such as the reflections from the horizontal-lying sediments, the fluctuation in the travel times of signals from a rough interface such as basement causes these reflection signals to add incoherently producing less than actual amplitudes for these signals. If the data that are averaged were collected in one spot-location rather than along a short section of a traverse, the second option might be superior.

Frequency effects

There are frequency dependent effects, and in order to reduce their significance, all data are filtered with a low frequency, 30 to 60 Hz, bandpass. The wavelengths range from about 20 to 90 meters in the sediments depending on the propagation velocity. The reflection of a signal having at least an octave bandwidth and long wave lengths is less subject to major amplitude changes due to interference effects resulting from closely spaced reflection horizons than narrower band and shorter wavelength signals. Absorption is low; and incoherent backscattering from sediment horizons is less than at higher frequencies because the magnitude of the horizon roughness is a smaller fraction of the longer wavelengths.

Integrand comparisons

In order to compare the integrands other than in the cursory manner of Figure 4, let us divide the integrand deflection into equal increments of cumulative energy and determine in descriptive terms how the increments may be related to the characteristics of the seabed. In the discussion of normalization we have pointed out the advantage of normalization relative to some reference horizon. If for instance the reference horizon were oceanic basement, we can divide the integrand into equal deflection increments relative to the integrand deflection immediately after the reception of the basement return and assign percentages to the increments relative to the "total" energy cumulated to this point. Thus we assume a synthetic series of equal energy steps and then examine ways to relate the reflected energy step-by-step to what

the physical characteristics of the seabed would have to be to cause each step.

The concept of generalizing the reflection integrand by representing it as a series of steps is perhaps unique. We rationalize this concept on the basis that the percentage values can be made small to fit an integrand having a number of discrete arrivals, and this approach simplifies the mathematical analyses.

We know rather well that the acoustic impedance of sea water at depth is about 1.6×10^6 rayls and of basaltic oceanic basement, about 16 to 18 $\times 10^6$ rayls. Therefore in our mathematical and physical analyses we seek to relate these equal energy percentile steps to changes in the acoustic impedance between these boundaries.

The equal steps of cumulative energy can also be calibrated in relation to the reflectivity of the sea floor once reflectivity is measured or assumed. The deflection of the first event of the integrands can then be made to represent the sound power reflection coefficient assuming the response of the seafloor is the same from shot-to-shot. Essentially this assumes that energy incident at the seafloor is unity and the first deflection some fraction (the reflection coefficient) of the incident energy. The cumulative energy at each integer multiple of the first deflection can then be measured relative to the coefficient thus again configuring an integrand of equal energy steps.

By assuming incident energy is unity, we are not dependent upon a knowledge of the shot-to-shot variation in seismic source level, but do depend in all these measurements upon a reasonable linearity in the response of the seabed to variations in incident energy. Baggeroer and Hoskins (1975) measured in a 10-400 Hz bandpass fluctuations of 2 to 6 dB in the source level of a 300-cubic inch airgun using a reference hydrophone 46 meters directly below the source. Knott et al (ibid) observed in a 20-120 Hz bandpass variations of 3 dB in the downward radiated energy from the 100 kJ underwater spark, measured 4.5 meters below the source in sea state 1 to 2. Figure 5 shows at two locations that the relative seabed response is quite repeatable for ten successive shots. This suggests linear response at least over the 2 dB range of the energies measured at the norm point of the original integrands from which this figure was produced.

Mathematical description of the reflection model

A quantitative analysis of the sequence of acoustic reflections from the seabed needs to begin with a logical and causal mathematical model. Although the model described here does not incorporate all the phenomena involved in the reflection and transmission through a sequence of seabed layers, it does provide an adequate identification of and an explanation for most of the received signal. We will first examine a steady state model and then show that geophysical realities allow major simplification of this model so that it is suitable for the case of transient signals. Since this mathematical model is based on a simplification of the actual situation, those geophysical features that appear to be of secondary importance and that can be neglected need to be stated.

The acoustic pulse travels from a source near the surface to the seafloor and returns to a receiver also near the surface and the source. The events of interest here are the reflections from the water-seabed interface and the reflections from within the seabed. The transmission path from the surface to the seafloor and the return path from the seafloor is virtually the same for all the reflections of one data set; the only difference in paths for these different reflections is within the seabed itself.

Within the seabed the sound is assumed to propagate as a plane wave. For deep sea seismic profiling the depth of the water is greater than the depth of penetration into the seabed. Thus, the transmission loss due to inverse-square spreading within the seabed is small and will be neglected for the purpose of this report.

The incident and reflected wave paths are assumed to be at normal incidence to the interfaces. The angles that do occur are so small that any corrections due to Snell's Law are much less than the resolution in travel time. Compressional wave propagation is assumed.

We assume the losses from scattering, absorption, and spreading within the water column are the same for all subject transmission paths. Variations in these common losses drop out by relating the reflection signals to one another in a relative

manner or to the sound incident at the water-seafloor interface by means of seafloor reflectivity measurements.

Within the seabed any losses due to absorption and scattering are assumed to be small in comparison to the effects due to the reflections. Both absorption and scattering are frequency dependent and are small for low frequencies, i.e. a 30 to 60 Hz bandpass.

Within a given layer the acoustic properties are assumed to be homogeneous and isotropic, with discrete, non-reactive interfaces. Further, we assume that the seabed responds linearly over the range of shot-to-shot variations in acoustic pressure generated by the seismic sources.

Implicit in the interpretations of measurements of reflected energy versus travel time is the ambiguity as to whether the reflections observed are due to an increase or decrease of impedance between succeeding layers. An overall increase in acoustic impedance with depth is to be expected, but there may be some impedance decreases or "inversions" interspersed. At the present we assume that there are no inversions. Analysis based on this assumption gives an upper bound but not a lower bound to the value of acoustic impedance versus depth (Fig. 6c).

Several factors enter into what produces changes in acoustic impedance and thereby a reflection. The most easily visualized geological structure is one made up of planar boundaries between materials of differing density and/or compressional wave velocity. In nature, boundaries may be discrete or transitional, or more specifically, discrete or transitional in respect to the bandwidth and wavelength of the signal insonifying it (Wolf,1937). One can also anticipate that the reflection wave train sequence observed will differ depending on the characteristics of the incident waveform. The smoothness, slope, and extensiveness of the interface also affect the manner in which it reflects sound.

For convenience in the development of the model we consider three separate situations for steady state waves: the first, a single interface, the water-seafloor reflector; the second, a basaltic basement with only one layer above it; and the third or general case, several layers between water and basement. The first situation is covered in acoustic texts (e.g. Kinsler & Frey,

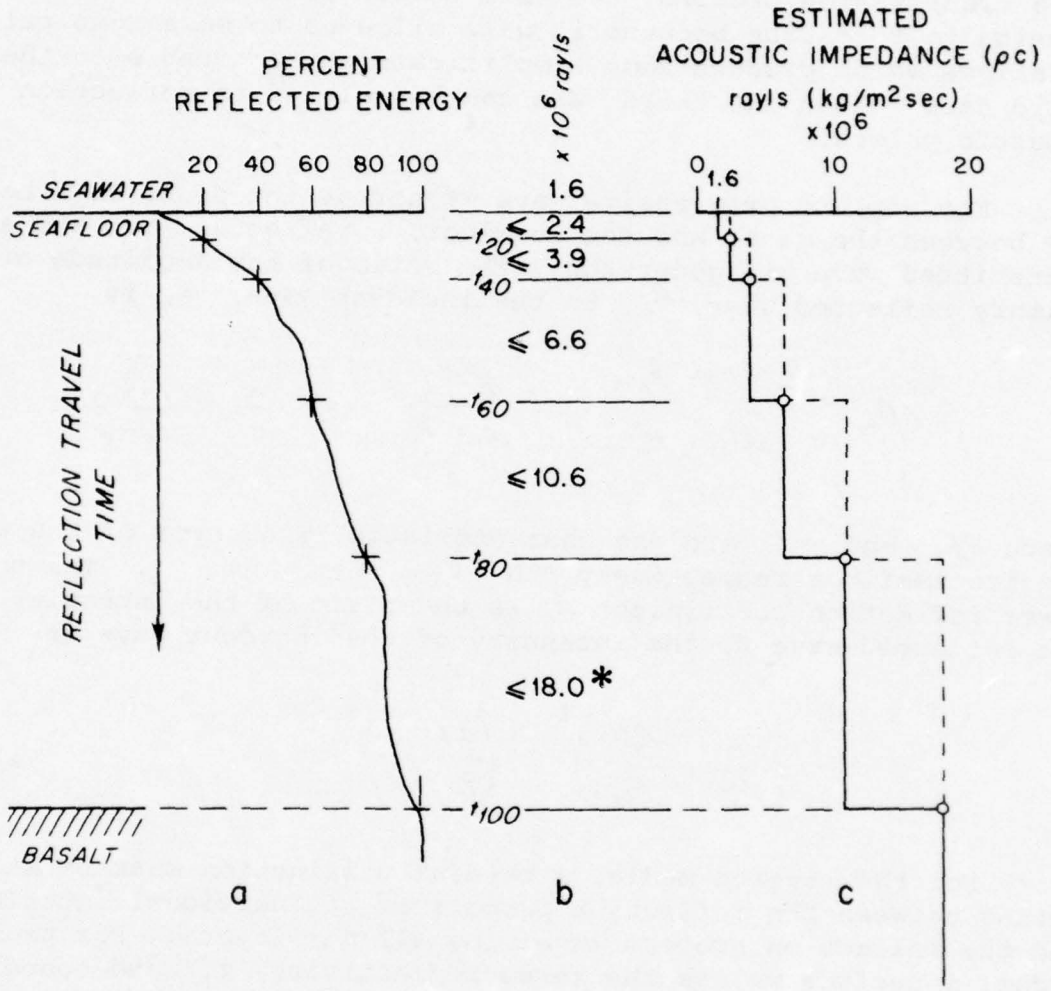

FIG. 6 Application of the five 20-percentile synthetic layer model to data.

(a) Cumulative energy curve re travel times to 20%, 40%, 60%, 80% and 100% of the energy cumulated up through reception of the basement return.

(b) Five synthetic layers with interfaces corresponding to each equal percentile step, labelled with maximum impedance predicted from model. (* 18.0 represents a high average, near maximum impedance for basalt.)

(c) Plot of estimated impedance vs travel time. The impedance is predicted to be between the solid and dashed line. Maximum values (dashed-line) are presented in all other figures.

1962). The second case is usually treated in texts (ibid p.136) as a transmission problem. We will devote considerable discussion to this case because it will allow us to make some calculations which produce some simplifications applicable to the third case. Then the third case can be related to reflection of acoustic pulses.

For a plane progressive wave at normal incidence on a boundary between the water and the seafloor, a reflected wave and a transmitted wave are generated. The ratio of the amplitude of the primary reflected wave, B_1, to the incident wave, B_0 is

$$B_1/B_0 = \frac{\rho_1 c_1 - \rho_0 c_0}{\rho_1 c_1 + \rho_0 c_0} = \frac{z_1 - 1}{z_1 + 1} \qquad z_1 = \frac{\rho_1 c_1}{\rho_0 c_0}$$

where $\rho_0 c_0$ and $\rho_1 c_1$ are the characteristic impedances of the water and the seafloor respectively and $z_1 = \rho_1 c_1 / \rho_0 c_0$. The sound power reflection coefficient α_1 is the ratio of the intensity of the reflected wave to the intensity of the incident wave or

$$\alpha_1 = \left(\frac{\rho_1 c_1 - \rho_0 c_0}{\rho_1 c_1 + \rho_0 c_0}\right)^2 = \left(\frac{z_1 - 1}{z_1 + 1}\right)^2 \qquad \text{Eq. 1}$$

For the layered media, a careful distinction must be maintained between the reflection process at an individual interface and the reflection process involving all the layers. For an individual interface we use the terms reflectivity, r, and sound power reflection coefficient, α (see Eq. 1). The effective sound power reflection coefficient for an entire sequence will be designated as the reflectance, $\mathcal{R}$, and it is defined as the ratio of the net intensity of the reflected wave to the intensity of the incident wave. For the case of only one interface, the reflectance is the sound power reflection coefficient or $\mathcal{R}_1 = \alpha_1$. For more than one interface, the reflectance depends on the sound power reflection coefficients of all the interfaces.

Next let us consider the second case when the incident plane wave from the water is transmitted through a finite layer into the third medium. When the incident wave arrives at the first inter-

face the wave is partly reflected and partly transmitted into the second medium. This transmitted wave continues until it arrives at the second interface. Here it is partly transmitted. The reflected wave returns to the first interface where again partial reflection and partial transmission into the water occurs. This transmitted wave combines with the wave initially reflected in the water, while the reflected wave combines with the wave initially transmitted, creating a steady state condition.

The wave amplitudes are summed with their proper phase relationship according to the Principle of Superposition for linear waves. The energy or the power is then computed from the resultant amplitude. The phase change, δ , between successive reflections is the same, 2π (path difference/wavelength), or $2k_1h_1$ where $k_1 = 2\pi/\lambda_1$, and h_1 is the thickness of the layer. The reflectance for the single layered seabed in terms of δ and the sound power reflection coefficients α_1 and α_2 is

$$R_2 = \frac{\alpha_1 + \alpha_2 - 2\sqrt{\alpha_1\alpha_2}\cos\delta}{1 + \alpha_1\alpha_2 - 2\sqrt{\alpha_1\alpha_2}\cos\delta} \qquad \text{Eq. 2}$$

(Details for the derivation of this equation are given in Appendix I).

The reflectance given in Eq. 2 is very dependent on the phase change δ . For a given thickness, the reflectance depends on the frequency. In optical applications and in most acoustical situations the calculations of the reflectance are made for a single frequency or a narrow band of frequencies. However, an important distinction must be made in the case we are dealing with, the signal is broad band covering at least one octave. Thus the effective reflectance that will be measured is the average over the frequency band. For typical values of α_1 and α_2, the product $\alpha_1\alpha_2$ in the denominator of Eq. 2 is very much less than 1 so it may be neglected. To simplify Eq. 2 for averaging over the frequency band, the denominator is expanded by the binomial theorem keeping terms on the order of α^2:

$$R_2 \approx \alpha_1 + \alpha_2 - 2\sqrt{\alpha_1\alpha_2}\cos\delta + 2(\alpha_1+\alpha_2)\sqrt{\alpha_1\alpha_2}\cos\delta - 4\alpha_1\alpha_2\cos^2\delta$$

But the average of $\cos\delta$ over the frequency band is zero while the

average of $\cos^2 \delta$ is 1/2. Thus the effective value of the reflectance to the level of α^2 for the broad band signal is

$$R_2 \approx \alpha_1 + \alpha_2 - 2\alpha_1\alpha_2 \qquad \text{Eq. 3}$$

In Appendix II a comparison between the average values of R_2 computed by Eq. 2 and Eq. 3 is made for values of $\rho_1 c_1 / \rho_0 c_0$ between 1 and 10 (where $\rho_2 c_2 / \rho_0 c_0 = 10$). This is equivalent to a variety of layers between water and the basaltic basement rock. The difference between the calculations from Eqs. 2 and 3 is less than the expected errors in the measured values of c and the reflectance.

Equation 3 can be simply derived another way. The averaging over the frequencies implies that the phase variations for broad band signals is not critical and hence we can deal with intensities directly. Also by keeping terms to the order of α^2 we need to consider the initial reflections and the first reflections of the down going rays only, i.e., returned energy from "multiples" can be ignored. Thus the intensity of the reflected signal will be the sum of the intensity of the signal reflected from the first surface plus the signal transmitted through the first surface reflected from the second and thence into the water again, or

$$R_2 = I_{refl}/I_{incid} \approx \frac{\alpha_1 I_0 + T_1^2 \alpha_2 I_0}{I_0} = \alpha_1 + \alpha_2 T_1^2$$

where T_1 is the transmission coefficient.

But $T_1 = 1 - \alpha_1$ so

$$R_2 \approx \alpha_1 + \alpha_2 - 2\alpha_1\alpha_2 \qquad \text{Eq. 3(a)}$$

This formulation will greatly simplify the calculations for the general case.

The general solution for the multi-layered seabed is more complicated. If the method outlined for Eq. 2 is followed (see Appendix I), each reflection generates an infinite series to be summed, quickly producing an unmanageable form. The other approach (see Fowles, 1975) is to set up a transfer matrix for each layer. Then the product of the individual matrices yields an overall transfer matrix from which the reflectance can be computed--again a difficult task for the general case. However, if the simplifications that allowed us to calculate Eq. 3(a) are used, the general equation for the reflectance is readily computed. The details are given in Appendix III. For four layers with five interfaces the total reflectance can be written as

$$R_5 = \alpha_1 + T_1^2\alpha_2 + T_1^2T_2^2\alpha_3 + T_1^2T_2^2T_3^2\alpha_4 + T_1^2T_2^2T_3^2T_4^2\alpha_5 \qquad \text{Eq. 4}$$

where α is the reflection coefficient between successive layers (Eq. 1) and T is the corresponding transmission coefficient. The subscripts designate the successive interfaces.

All of the preceding analysis is based on a steady state solution while the experimental signals are broad band pulses. However, the conditions which permitted us to write Eq. 4 are equally applicable for broad band pulses. Averaging over a frequency band essentially decouples the phase variations for the steady state calculation; the same should be true for pulse operation. By keeping terms to the order of α^2 only, the multiple reflections are assumed to produce a negligible contribution to the received signal and therefore the reflection from each interface is independent of the other reflections. The analysis used for Eq. 4 should apply equally well for pulses. In other words the total reflected signal can be considered to be the sum of a sequence of independent reflections from successive interfaces (Appendix III); hence the use of the cumulative energy curve.

For computational purposes we have initially structured our model to represent the acoustic impedance contrasts that would cause five equal (20%) energy increments (Fig. 6). The intervals then in effect become synthetic equivalent acoustic impedance steps, or generalized "horizons" between generalized "layers". The increments in travel time and hence the apparent thickness of

the generalized layers depend on the shape of the observed cumulative energy curve, Figure 6a. The impedance modelled in our study area is constrained by relatively well known boundaries, at the top of the sediment column by the impedance of seawater and at the bottom by that of basaltic basement. Energy percentiles on the cumulative energy curve range therefore from zero at the onset of sediment returns to 100% after reception of the basement return.

The model is applied in two ways, and four conditions control its effectiveness for estimating the acoustic impedance structure with depth. In the first, the model predicts a series of impedance value steps for each 20% step in cumulative energy. In the second it predicts a series of impedance steps for integer multiples of the sound power reflection coefficient, α , in terms of reflectance. Effectiveness is controlled by:

1. Where there are both a return from basaltic basement and a determination of seafloor reflectivity, the model can be applied both ways for comparisons.

2. Where there is a basement return, but no reflectivity measurement, the first method is applied.

3. Where there is no discernible basement return, but reflectivity is measured, the second method is applied. The first may be used as an approximation, but a lesser impedance value than that of basalt must be assumed for the terminal value of the cumulative energy trace.

4. Where there are neither a basement return nor a reflectivity measurement, relative impedance variations can only be estimated on the basis of geological or reflectivity and reflectance assumptions.

The reflection model can be used to estimate the impedance structure and to establish a base from which to measure anomalous changes witnessed in the reflection energetics. Even if the model is not precise it can thus provide a basis for comparisons between the energetics observed in different areas.

Impedance re reflectance

In order to work with equal steps of cumulative energy the

reflected contributions from each interface defined in Eq. 4 must be made equal(Figure III-1, Appendix III). In Eq. 4 the second term ($T_1^2\alpha_2$) is made equal to the first (α_1), the third ($T_1^2T_2^2\alpha_3$) equal to the second ($T_1^2\alpha_2$) and so on. In this way by starting with an appropriate α_1 or sound power reflection coefficient for the seafloor we can solve for the successive α's. Then the impedance contrasts and subsequently the impedances can be derived from Eq. 1. A family of curves is then generated by substituting a range of α's which gives the acoustic impedance of each synthetic equivalent layer and the number of synthetic layers to be expected between the seawater and basaltic basement (Fig. 7 and 6).

The logic is reversed to relate impedance to the percentage of total reflected energy. The impedance of the 5th 20-percentile synthetic equivalent layer has then to be considered in terms of the maximum it will reach in that interval, terminating at the bottom of the layer with an impedance of basalt (dashed line in Fig. 6c). Further, the reflectance of the first layer is not equivalent to the sound power reflection coefficient of the seafloor as above, but rather a synthetic α for the entire first synthetic equivalent layer. In this case the impedance of each synthetic layer is read off that ordinate in Figure 7 where the line signifying the 5th layer crosses an appropriate terminal value of impedance for basalt (16 to 18 x 10^6 rayls).

Impedance structure can therefore be estimated rather easily from much of the conventional deep-sea seismic profile data. Basement returns are commonly received, and the extent of the oceans where water-column multiples do not interfere is great.

Use of the seafloor return as a reference horizon has the advantage of an omni-present reference, but the added complications associated with seafloor reflectivity measurements are necessarily involved. Reflectance based upon seafloor reflectivity is particularly useful for assessing the reflected energy budget, because the deflection at any point of the integrand scaled to the sound power reflection coefficient equals the reflectance at that depth or travel time. With such calibrated curves we can refer to the "sediment reflectance" (reflectance to the base of the sediments) or the "basement reflectance" (total reflectance to just after reception of the basement return).

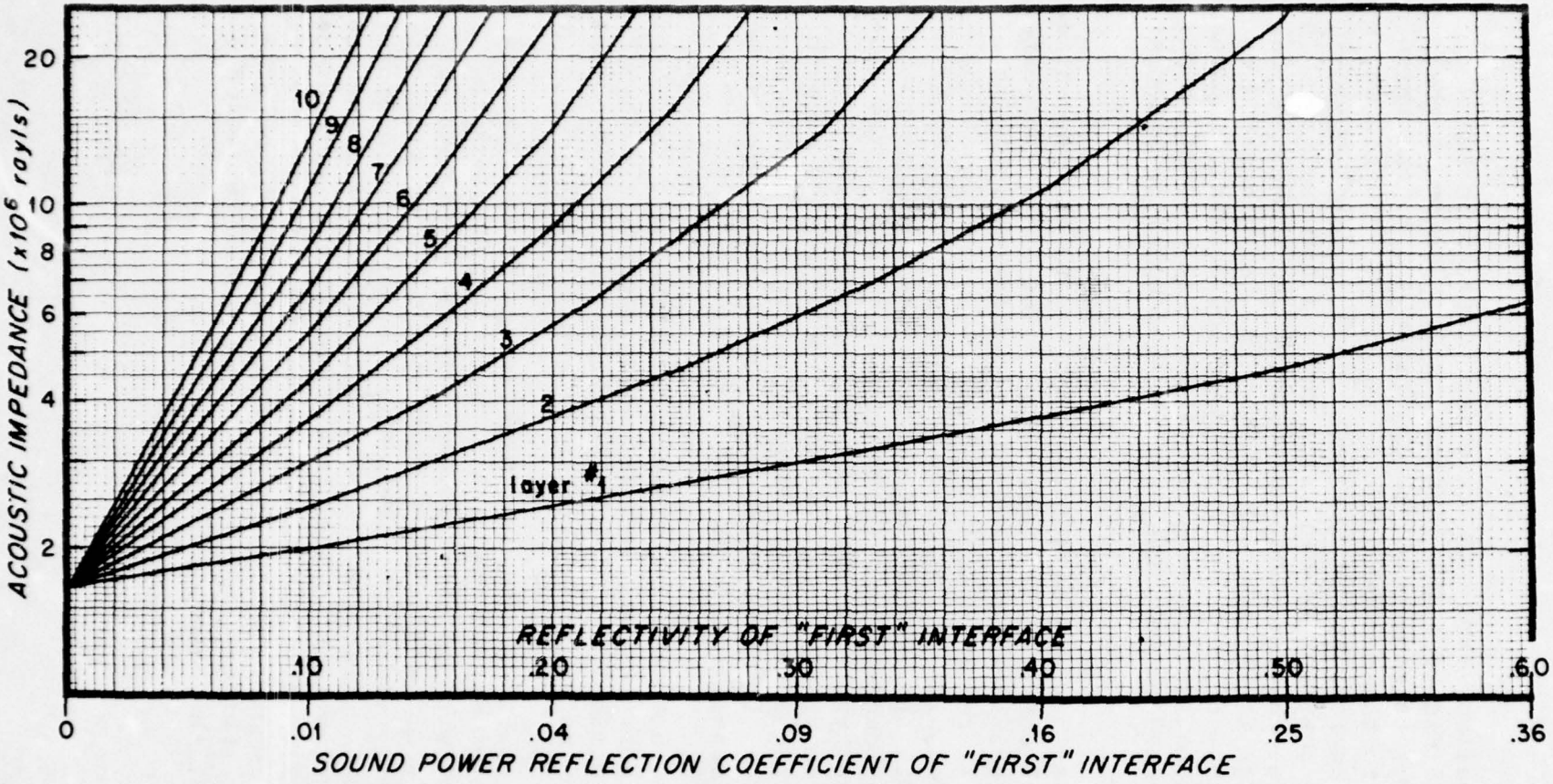

FIG. 7 Model prediction of the acoustic impedance of 10 synthetic layers, each interface causing reflections of equal energy as observed in the water layer. Plotted as a function of the sound power reflection coefficient and reflectivity coefficient of the "first" seabed interface. When the 20-percentile method is used, the "first layer" extends from the seafloor down to t_{20}. The impedance of this first layer may or may not be equal to that of the seafloor.

Measurement uncertainties

In each approach, either via reflectance or percentage, it is necessary to consider and define what constitutes the return from the reference interface. This need is best demonstrated by the reflectance measurements based on seafloor reflectivity. If the sound power reflection coefficient is already known, the question is, at exactly what point on the integrand does the deflection equal the coefficient? We define this point in time from the onset of returns to be equal to the "effective pulse length" of the seismic source. If this time is picked too early or too late, the deflection will be too low or too high and this will cause subsequent scaling errors in reflectance. Reasonable comparisons of reflectance can be made if such an error is consistent because the error approximates a coefficient applied to each reflectance that is compared. Estimates of impedance, however, will be greatly distorted (Fig. 8). Concerning basement as a reference, it is unusual when the relief in travel time along a profile is not several times the period of a basement return, but at a station a sequence of shots can usually be selected in which the migration of the basement return is minimal.

The "effective pulse length" includes the effects of the multi-path sea-surface reflections at the source and receiver upon the characteristic pulse length of the source. We have estimated the effective pulse length for these data to be 50 to 80 milliseconds, and when dealing with the basement return we have extended the period to 100 ms to allow for some travel time variation. The source in this case was the combined output of a 100 kJ underwater spark and a 10-cubic inch airgun synchronized to the first positive pressure pulse while each was towed at about the same depth (8 to 9 meters). A 50 millisecond effective pulse length is appropriate for the spark and the towing geometry of the source and receiver. The effective pulse length of the airgun is not so easily defined because of the many oscillations of the bubble pulse train (period of one oscillation is 40 ms for this size gun). In this bubble pulse train the acoustic pressure of the first bubble pulse is roughly 6 dB less than the initial pulse, and at this towing depth destructive interference caused by the surface reflection further reduces the contributions from all the airgun bubble pulses. Hence we have estimated that the oscillations are reduced to a relatively insignificant level by the end of a 80 millisecond period.

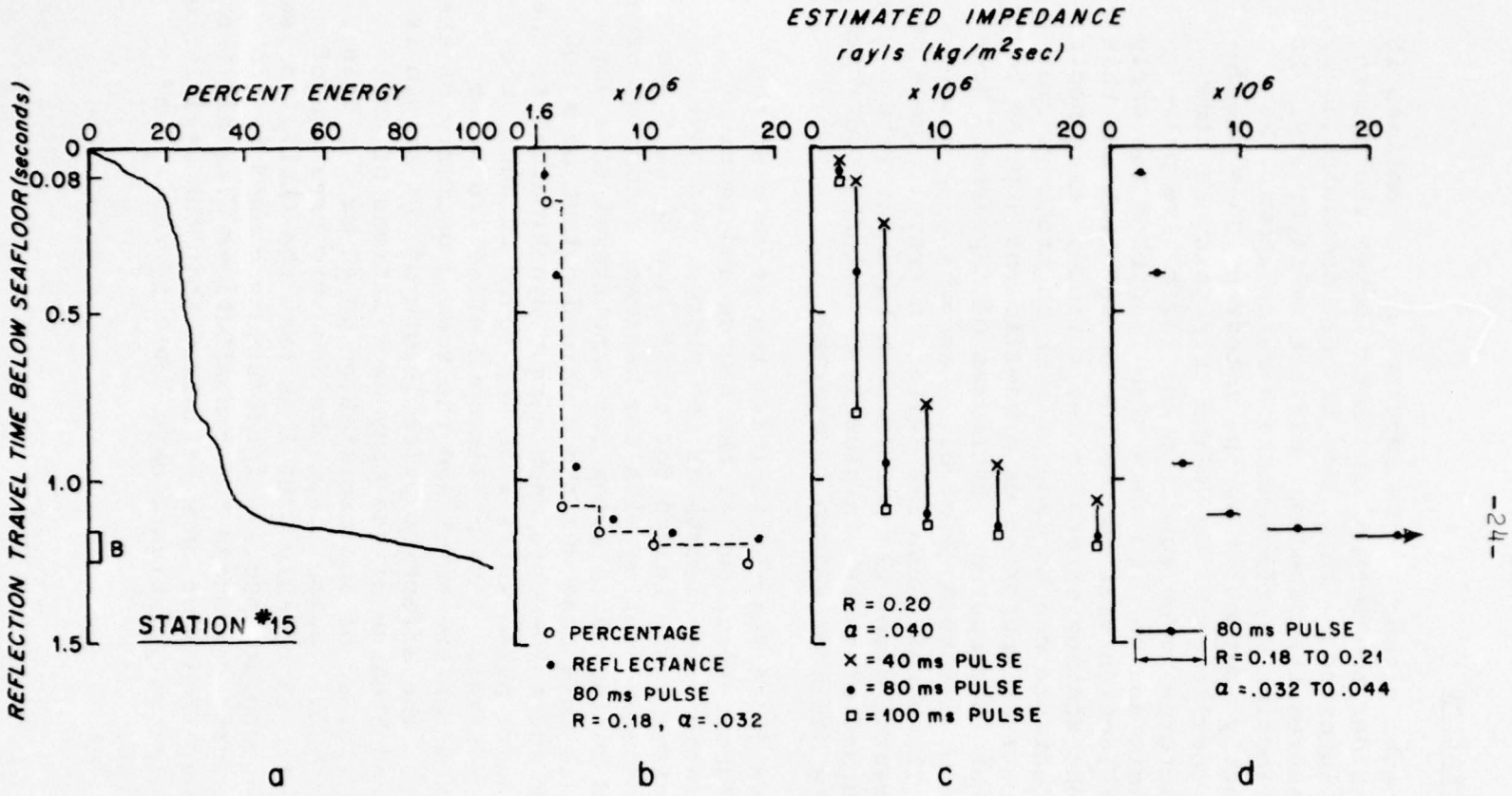

FIG. 8 The effects upon impedance estimates due to variation in effective pulse length and the sound power reflection coefficient of the seafloor.
(a) The reflection integrand of station #15 (expanded scale). Basement is indicated.
(b) Impedance estimates based on the 20-percentile and reflectance applications of the model. A pulse length of 80 ms and a sound power reflection coefficient (α) of 0.032 from the 30 to 60 Hz reflectivity measurements combine to produce this "best" fit.
(c) The effect of pulse length on the impedance estimate.
(d) The effect of variation in the determination of α on the impedance estimate.

Seafloor reflectivity and signal-to-noise ratio

The most straightforward way to determine the reflectivity or the reflectance is to compare the initial or total returns with the incident signal, but this requires measurement of the incident waveform. Since this was not done we are obliged to determine reflectivity indirectly. A credible measurement of the reflectivity coefficient is obtained by determining the ratio of the amplitude of the initial event in the first water-column multiple of the seafloor reflection to the amplitude of the initial event in the directly received seafloor reflection, allowing for a factor of two for transmission loss and assuming sea surface reflectivity to be 100%.

With a favorable signal-to-noise ratio, reflectivity could be so determined by computer from the returns of each shot, but in the subject data the signal-to-noise ratio of the initial arrival of the first water column multiple is typically 1 dB. If the signal-to-noise is less, the deflection of the amplitude trace can only be estimated and the magnitude of the integrand becomes indeterminable (Appendix V). To improve reflectivity measurements particularly in the 30-60 Hz bandpass we increase the signal-to-noise ratio 4 to 6 dB by averaging an appropriate number of amplitude traces and processing the resulting waveforms.

Since the frequency spectrums of the signal and the noise are different, the signal-to-noise ratio is better in some frequency bands than others. For these data the 240-480 Hz bandwidth appears optimum. Reflectivity measurements were determined in this band, in the 30 to 60 Hz band and other octave bands.

Reflectance along reflection profile traverses

The continuity or transitions in physical character of the reflection horizons evidenced by changes in reflectance along tracks crossing different geological provinces are of particular interest. To portray these changes we construct an overlay to the familiar reflection profile record, consisting of contours of the reflection integrand of each successive shot (Figs. 9 and 10). The integrands, and thus the contours, are normalized as before to a reference horizon or reference travel time and presented in terms

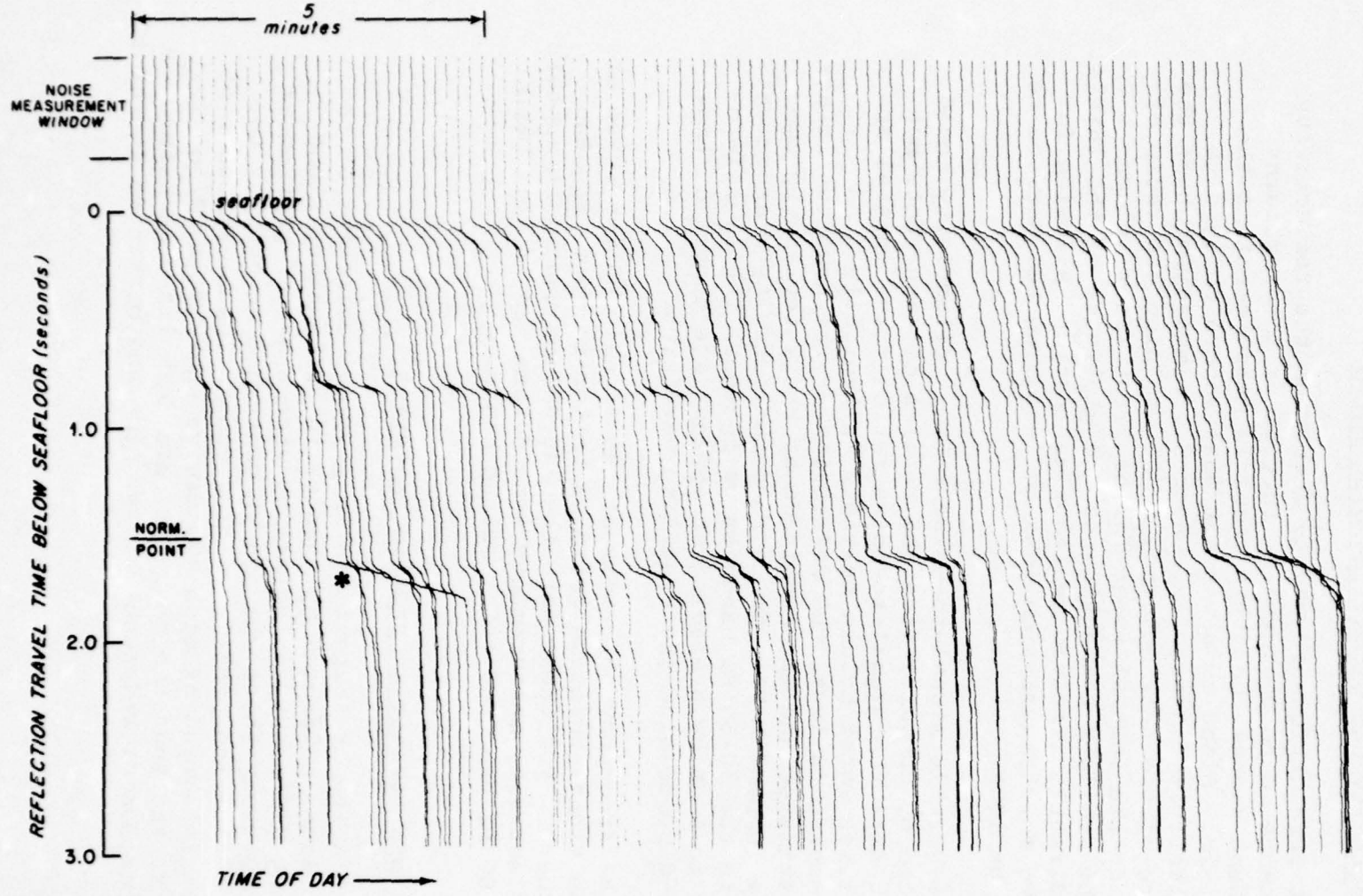

FIG. 9 Successive shot-by-shot cumulative energy integrands from station #3. Mid-sediment norm point and noise sampling window are indicated. Such a set of integrands is derived from the pressure-time curves and contoured (Fig. 10). Repetition period between shots is 10 seconds; ship's speed, about 6 knots. (* identifies same shot, Fig. 10)

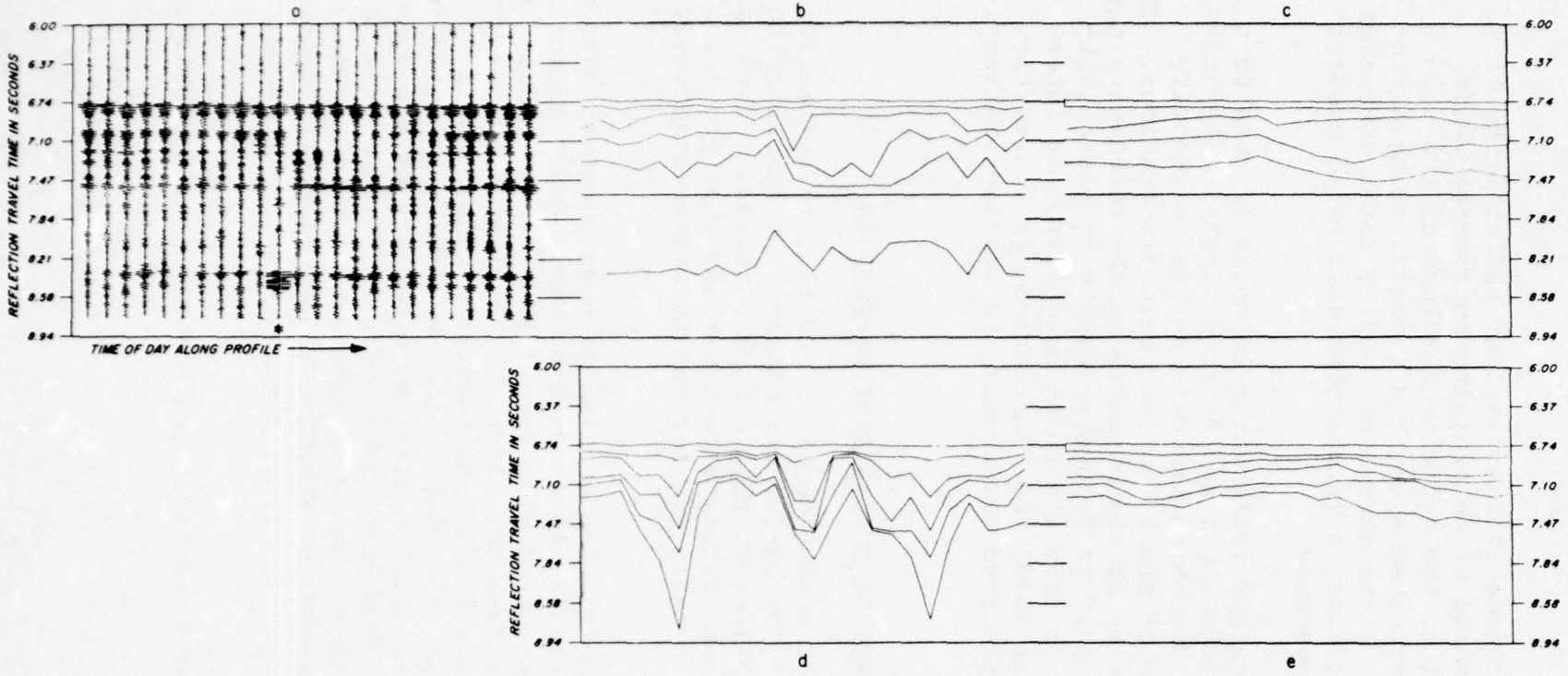

FIG. 10 Twenty-four pressure-time curves from the same sequence as Figure 9,(a), and contours of the integrands from Figure 9, Station #3. (* identifies same shot, Fig. 9)

(b) Contours of cumulative energy at 0.2, 0.4, 0.6, 0.8, 1.0 and 1.2 of the energy-value measured at the norm point, 7.6 seconds.

(c) Same as (b) but contours are smoothed with running-average "low pass" filter.

(d) Contours of cumulative energy in terms of reflectance using multiples of the seafloor return measured at 50 milliseconds from the onset. - Uniform seafloor reflectivity assumed.

(e) Same as (d) but contours smoothed with running-average "low-pass" filter.

of percentage, or reflectance if the seafloor reflectivity is known or estimated. Instead of determining an average-shape integrand as for a station, the deflection values of the successive integrands are smoothed along the traverse using a running average algorithm. Although one can easily infer estimated impedance from these profiles, a future step will be to present contours of estimated impedance.

Both the percentage and reflectance contours of data that have not been smoothed (Fig. 10 b and d) show significant variations in travel time. Smoothing the data serves to identify the relative proportions of short and long term fluctuations. The fluctuations in travel time of the contours in the cumulative energy curve in Figure 10(b) appear to be due primarily to variability in the strength of the return from the reference horizon at intermediate depth. In Figure 10(d) the fluctuations in travel time are apparently due to localized variability in seafloor reflectivity.

Possible criteria for mapping seabed characteristics

We propose a set of measurements in addition to reflectivity and reflectance which may be useful for mapping the characteristics of the integrands from different physiographic regions. These are objective rather than interpretative observations that provide a relatively quick and systematic way for making areal comparisons.

Seabed time constants: The cumulative energy curves have a shape that is somewhat similar to a charging curve for a capacitor. One characterization associated with such curves is the "time constant", the time to rise from the onset of the first seafloor arrival to some specified fraction of its terminal value. For a generalized time constant characterization we suggest two time intervals, t_{20} (time period for 20% rise) as a measure of the seafloor response, and t_{80} (80% rise) as a measure of response time of the entire return. These time constants are frequency dependent, hence the passband must be specified. The time constants at low frequencies are usually longer than at higher frequency passbands.

For reflection sequences including a strong but variable re-

turn such as from basaltic basement, an average integrand should be used. The contoured profiles are helpful in choosing a representative group of reflection sequences for averaging. The time constant is also affected by the relative proportion of the total return from the sedimentary and from the crystalline rocks (Appendix IV). Should one wish to consider just the sedimentary sequence, the time constants (as a function of frequency) of the sedimentary portion of the integrand may be more meaningful than the entire return.

Shape of the energy integrands: The general shape of the cumulative energy curve is another feature for characterization. Two extremes of this curve are a "tread" function and a "step" function. In the first case very little energy is received followed by a terminal brust of energy. In the other extreme the energy rises initially very fast to almost 80% and then gradually approaches 80% at t_{80} giving a single step-like trace. An intermediate case is a simple ramp function, the cumulative energy increases linearly with time giving a straight line from zero energy at t = 0 at the onset of arrivals to 80% at t_{80}.

To obtain a measure of this shape, we define the term "$Area_{80}$" which is the ratio of the area under the energy-time curve divided by the area under the simple ramp function to the time t_{80}. For computational purposes we use the trapezoidal approximation obtained by dividing the time into intervals corresponding to the energy levels of 20, 40, 60 and 80 percent.

This application yields the equation

$$Area_{80} = 1.75 - (t_{20} + t_{40} + t_{60})/(2\ t_{80})$$

With this definition the values for $Area_{80}$ should range from 0 for a tread function, passing through 1 for the ramp function, to 2 for the step function. This approximation actually yields values between .25 and 1.75. This discrepancy is not serious since the values of $Area_{80}$ are for classification and comparison purposes. So long as the method is consistently used, the gross comparisons can be useful. Figure 11 displays the relationship between estimated acoustic impedance and $Area_{80}$.

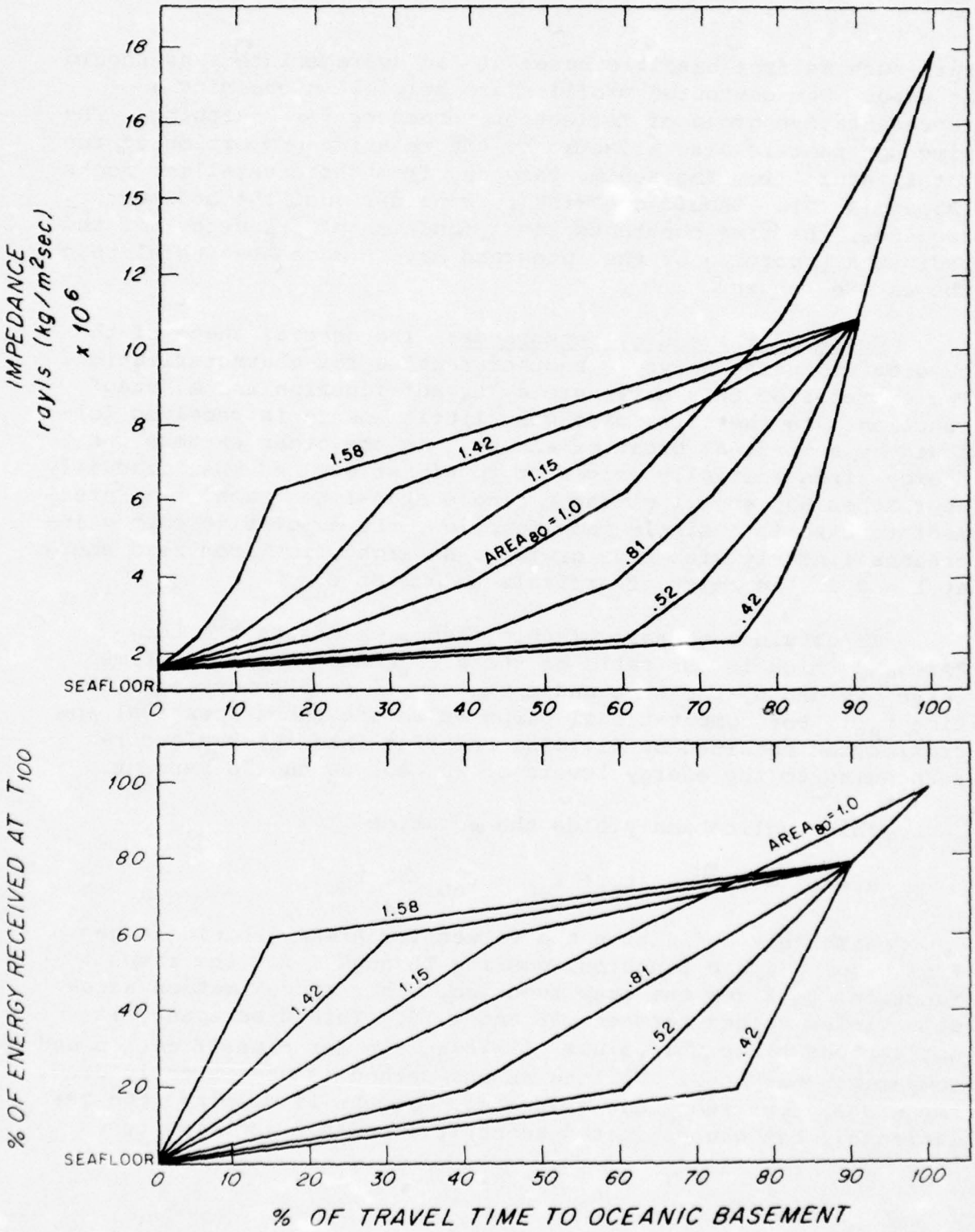

FIG. 11 Relationship between the numerical value of $Area_{80}$ and the estimated impedance.

Data handling

The normal incidence reflection data are taken from analog magnetic tape recordings collected in the field at sonobuoy stations. The longest taped profile is therefore about 20 km. The shipboard receiving and tape recording systems that were used are linear over a dynamic range of about 40 dB over a bandwidth of 10 Hz to 3 kHz.

Data from the tapes are digitized using two methods to control the digitizing rate. In the first we expect from timing calibrations that the time fluctuations of the tape drive will be minimally cumulative, and will not exceed the order of 0.01 second in the period of the 6 to 7 second reflection travel time. In this case a separate clock drives the digitizer at 2000 Hz. This procedure has appeared adequate for examinations of the reflected energy curves from the first seafloor reflections, but becomes tenuous when exact timing of the first water column multiple of the seafloor return is sought for reflectivity measurements. In the second method the digitizing rate is controlled by a signal (960 Hz) derived from the original time base of the experiment(60Hz) that was tape recorded with the data.

Data digitized by either method are analyzed via our programs using a 32,000 word Hewlett-Packard 2100 computer with two 1.2 million-word discs, two 9-track magnetic tape drives, a CRT terminal, an incremental plotter and line printer (Prada, 1976). To assure the validity of the energy measurements, the program outputs were calibrated by using digitized known signal inputs. Bandpass filtering was controlled by calibrated analog (Allison, Model 2-AR) filters because the symmetry of their response was better than we were able to produce by simple time-domain digital filters.

RESULTS AND DISCUSSION

The Data

We have examined tape recorded normal-incidence reflection data taken concurrently with wide angle sonobuoy profiles from six sites (#3, #4, #8, #14, #15, #17, Fig. 1). Two adjacent stations #3 and #4 provide a means to check the repeatability of results and one station, #14, is only 30 km from DSDP site #235. On the original

reflection profile record there is good evidence for the continuity of the reflection horizons between the drill hole site and station #14, that provides a reasonable basis for correlation of data from these two locations.

Similarities and differences between the sediment structure at the stations are apparent in short sections of the reflection profiles (Fig. 3), and the sediment thickness in reflection travel time is seen to vary from about 0.3 to more than 2.0 seconds. Ridges and other basement outcrops in the region are purposefully avoided (Fig. 3(b)). Water depth for all stations is about 5100 meters. Depth to oceanic basement obviously varies and at #8 basement is not detected below a deep and relatively strong reflector. Roughness of the sedimentary horizons appears to be minimal, but various degrees of roughness are exhibited in the basement returns.

Seafloor reflectivity

Reflectivity was measured in various octave bandwidths particularly at station #3 to see if the determinations could be refined (Table I). The average of all reflectivity coefficient measurements is 0.195, the mean 0.209. There is an upward trend with increase in frequency which is amplified by squaring to obtain the sound power reflection coefficient. The reasons for this trend are not clear and cannot be resolved with the data at hand. The trend could quite possibly be caused by the fact that the time period from the onset of arrivals which determines the measurement point is held constant, while in reality the effective pulse length may become shorter with increase in frequency. Or the trend may be indicative of an effect of surficial reflection horizon spacing as a function of frequency. A value of 0.20 appears to be a reasonable representation of the reflectivity coefficient for the region.

A number of piston cores which penetrated the sediments 1 to 10 meters have been obtained in the Somali Basin environs during four Woods Hole cruises (Table II). The upper sediments recovered were primarily calcareous ooze or calcareous siliceous ooze which indicates a degree of uniformity of the water-sea floor interface throughout the region. From these samples, we anticipate the uniformity found in the reflectivity of this interface.

TABLE I

Frequency		Station Number 3		4		8		14		15		17	
		Range*	Mean	Range	Mean	Range	Mean	Range	Mean	Range	Mean	Range	Mean
Reflectivity	30-60 Hz	.18	.18	.17	.17	.14-.23	.184	.12-.23	.176	.12-.17	.145	.14-.23	.184
	120-240	.15-.27	.209	------		------		------		------		------	
	180-360	------		------		.17-.28	.226	------		------		------	
	240-480	.15-.39	.226	.16-.27	.214	.17-.26	.214	------		.17-.30	.235	.17-.20	.189
	360-780	.19-.24	.214										
	960-1920	.24?	.24										
"average" Reflectivity			.213		.192		.208		.176		.189		.186
"average" α			.044		.037		.043		.031		0.36		.035
Relative reflectance (a) to base of sediments			5.7		5.7		5.9		2.3		5.4		2 or 6 !
Relative reflectance (b) including basement			7.5		6.2		5.9 !!		10		13		16
Sediment reflectance		.25 - .23	(.044)(.040)	.21 - .23	(.037)(.040)	.25 - .24	(.043)(.040)	.07 - .09	(.031)(.040)	.19 - .22	(.036)(.040)	.07 - .08 or	.21 - .24
Basement reflectance		.33 - .30	(.041)(.040)	.23 - .25	(.037)(.040)	.25 - .24	(.043)(.040)	.31 - .40	(.031)(.040)	.47 - .52	(.036)(.040)	.56 - .64	(.035)(.040)

* upper and lower quartile range of reflectivity measurements, about nine samples.
single numbers are from the average of 10 amplitude traces to improve S/N ratio.

** computed using α = the square of the average of the median Reflectivity at each station (first paren), as well as α = .04 for Reflectivity = .20 (second paren).

! depending upon interpretation of transition between sediments and basement.

!! near basement.

"average" α : determined from both the single number and median of each reflectivity range.

Table II

Sediment cores in study area 0°-10°N, 51°-58°E
(abstracted from WHOI Geological Samples Data File)

Location (°N, °E)		Depth (corrected meters)	Sediment Description	Cruise
09.11	052.24	4499	calcareous, irregular contacts, extensive mottling, uniform lithology	AII 15-4
09.02	053.40	4852	calcareous ooze, irregular contacts	AII 15-4
08.59	054.47	4950	calcareous ooze, volcanic glass, sharp contacts, mottling, uniform lithology	AII 15-4
08.58	052.02	4350	siliceous clay, irregular contacts	AII 15-4
08.58	052.20	4722	siliceous clay, irregular contacts	AII 15-4
08.58	056.02	4001	calcareous ooze	AII 15-4
08.54	051.37	3797	calcareous ooze, volcanic glass, uniform lithology	AII 15-4
07.54	055.58	4250	calcareous ooze, gradational contacts, extensive mottling	CH 100-4
07.52	054.46	5102	calcareous siliceous ooze	CH 100-4
07.48	056.12	4680	calcareous siliceous ooze, extensive mottling	CH 100-4
07.44	054.46	5102	calcareous ooze, gradational contacts, cross bedding	CH 100-4
07.04	055.58	4250	calcareous ooze, gradational contacts	CH 100-4
06.55	054.42	5106	foraminiferal sand, sharp contacts, cross bedding	CH 100-4
05.55	051.38	5114	calcareous siliceous ooze	CH 43-1
05.52	053.51	4944	calcareous ooze-clay	CH 43-1
05.22	054.33	4864	calcareous ooze, gradational contacts	CH 43-1
04.27	051.08	5049	calcareous ooze, sharp contacts	CH 100-4
** 03.14	052.41	5123	calcareous ooze, sharp contacts, cross bedding	CH 100-4
* 03.08	052.38	5126	calcareous siliceous ooze, sharp contacts, cross bedding	CH 100-4
* 02.55	055.43	3697	calcareous ooze, uniform lithology	CH 43-1
01.57	053.59	5126	siliceous calcareous ooze	CH 100-5
01.49	056.52	4782	unfossiliferous clay-calcareous ooze, sharp contacts	CH 100-5
01.38	053.20	4787	calcareous siliceous ooze	CH 43-1
01.05	053.30	5104	calcareous siliceous ooze, cross bedding	CH 100-5
00.56	053.18	3561	siliceous ooze, unfossiliferous clay, cross bedding	CH 100-4
00.14	056.04	4576	foraminiferal sand, sharp contacts, cross bedding	CH 100-4

**at and * near DSDP Site # 235

We have based some of the later comparisons on this reflectivity (0.20), a sound power reflection coefficient (α) of 0.04, and an effective pulse length of 50 to 80 milliseconds with full realization that these values may vary.

Reflectance

Sediment and basement reflectance in Table I are all based on an effective pulse length of 50 milliseconds, but on three α's: the standardized 0.040; the "average" α at each station (the square of the "average" reflectivity); and the α measured in the 30-60 Hz band. These are plotted in Figure 12. Note, that these reflectance comparisons are made without reference to impedance estimates. The choice of a 50 millisecond effective pulse length as a basis for this set of measurements causes the reflectance to increase too rapidly in too many steps to be accomodated by the nomograph in Figure 7. A longer effective pulse must therefore be inferred. Further, the use of the cumulative energy curve precludes assessment of impedance inversions--reflected energy is added on an absolute basis regardless of phase.

With these limitations in mind, this plot (Fig.12) shows that sediment reflectance increases and basement reflectance decreases with increase in sediment thickness. The difference between the sediment and basement reflectance measurements (see p.21) for the three stations #17, #14, and #15 to the south and southeast of the Basin proper is consistently greater than at the other three stations. For shallow basement and thin sediments this can be expected. Yet at #15 the thickness of sediment is almost equal to that at #4, but the large sediment/basement reflectance difference persists at #15 and does not occur at #4, nor at #3 and #8. This suggests that there is an entirely different depth-distribution of impedance in the southern part compared to the northern part of the region, a difference that will be more apparent when the individual stations are discussed.

The general decrease in basement reflectance with increase in sediment thickness is indicative of an impedance matching phenomena in which the sediments between the low impedance water and high impedance basalt act as a transmission coupling network (Appendix IV). A chance distribution of impedances within the

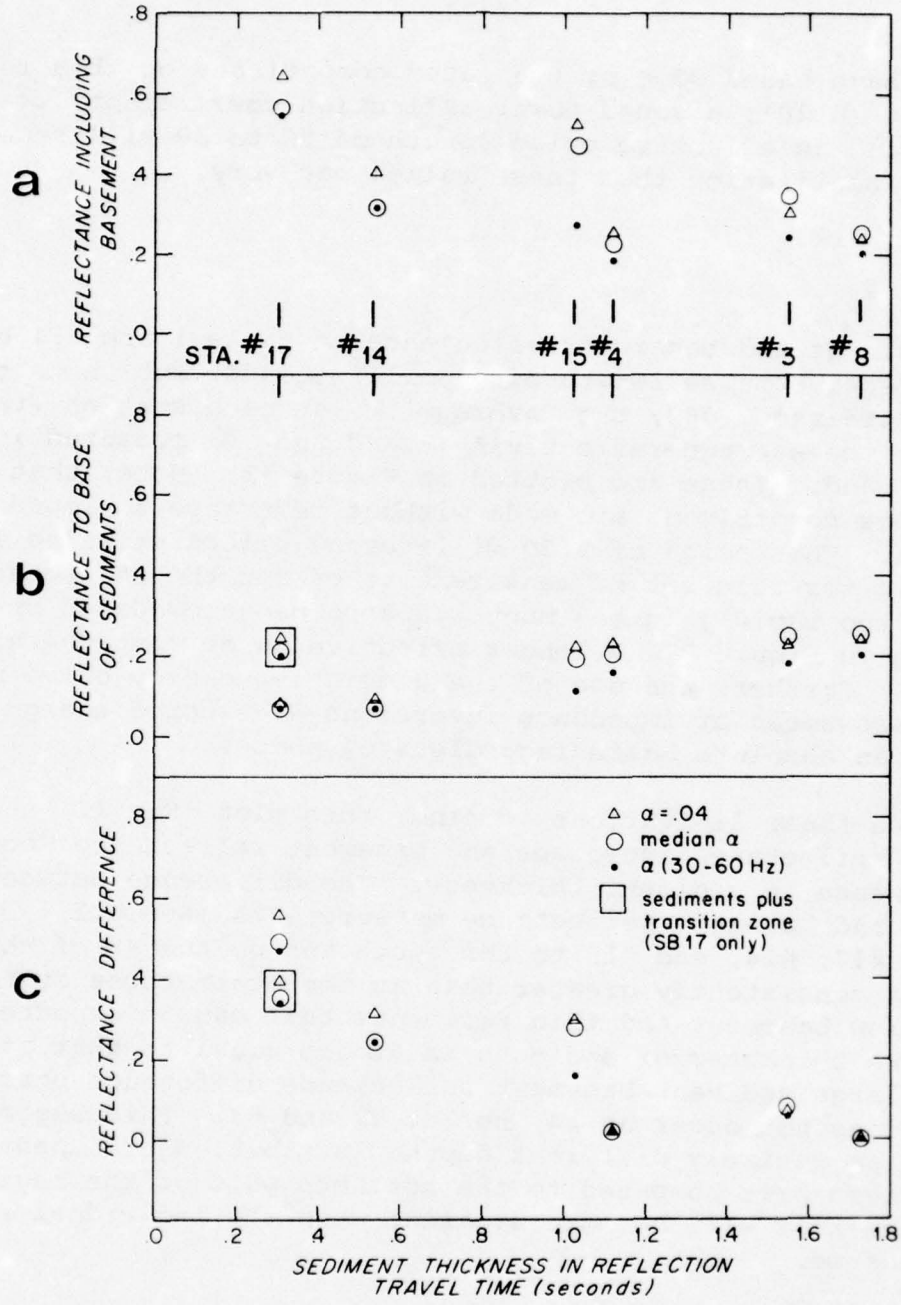

FIG. 12 Sediment and basement reflectance as a function of sediment thickness above oceanic basement. (Based on effective pulse length of 50 milliseconds).

(a) A general downward trend in basement reflectance with increasing sediment thickness is evident.

(b) Sediment reflectance does not increase so rapidly with increase in thickness as basement reflectance decreases.

(c) Difference between basement reflectance and sediment reflectance suggests an impedance gradation in depth at stations #4, #3 and #8 that reduces basement reflection and optimizes transmission coupling into basement.

sediment may satisfy to a degree the gradation of impedance required between the two bodies of contrasting impedance for optimizing transmission into the basalt from the water. Apparently the distribution is optimized moreso at #4 than at #15.

It has been recognized (E.T. Bunce, G.M. Purdy, personal communication) in deep sea refraction studies that the energy from shots appears to couple or transmit better into oceanic basement when sediments are present than when not. But we do not intend to account for the energy budget losses due to absorption, spherical spreading, scattering etc. required to obtain a true estimate of normal incidence transmissivity. Within the framework of our assumptions we can deal with reflectance and recognize its relationship to transmissivity.

The stations

Figures 13 and 14 show estimated impedance structure at each station, the data from which the estimates are derived, and the interval velocity profile determined at the location. The section of the normal incidence profile that the integrand represents is indicated; the amplitude squared trace is presented to identify discrete reflection horizons and the basement return. Estimated impedance graphs display the maximum impedance within each synthetic layer computed from the 20-percent energy steps measured relative to the cumulative energy of the basement return.

In Figure 13 (stations #3, #4, and #8) we present impedance estimates based both on percentage and on reflectance. In Fig. 14 the estimates based on reflectance are omitted, because they are for the most part presented in Figure 8 (page 24) and in Figure 15.

The most obvious differences in the station data are the energetic responses and estimates of impedances of the sediment in the two sets of data as grouped in Figure 13 and 14. After the initial return the integrands of #3, #4, and #8 have a series of small steps up to and including basement, whereas at #14, #15 and #17 there is an initial sediment response but little energy cumulated until a strong return from basement is received. The impedance steps are near linear in the first group and are "tread-like" in the second. These differences seen on the curves are

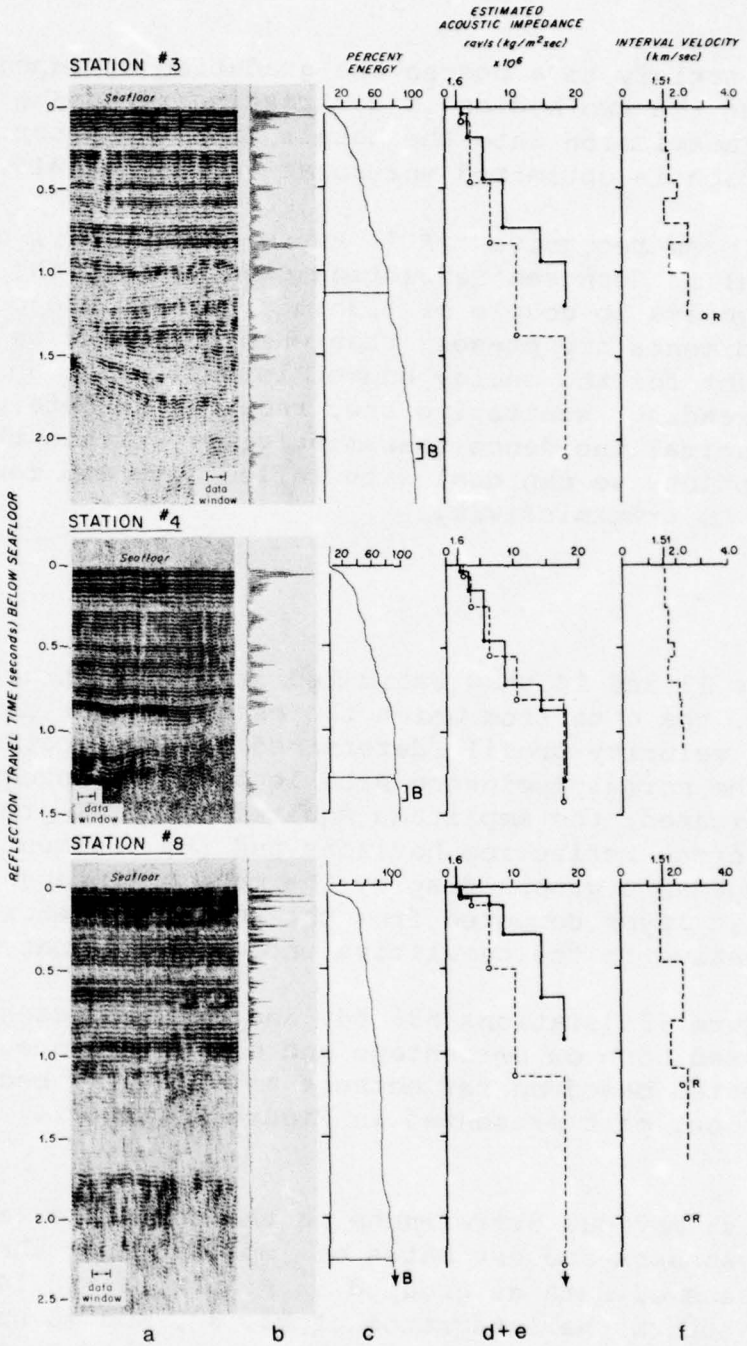

FIG. 13

Stations #3, #4, and #8 - estimated impedance structure with depth; the seismic reflections from which the estimates are derived; and interval velocity.

(a) 3.5 km section of the normal incidence profile at station.
(b) Amplitude-squared trace of one reflection from data window.
(c) Average-shape cumulative energy curve derived from reflection traces of data window, normalized to a standard unit deflection where indicated. Duration of basement return indicated by bracket.
(d) Estimated acoustic impedance based on 20-percentile application of model (dashed-line) and (e) estimated impedance based on reflectance using a 50 millisecond effective pulse length and $\alpha = 0.04$ (solid line).
(f) Interval velocity profile determined at station (o, R = critical refraction velocity determinations).

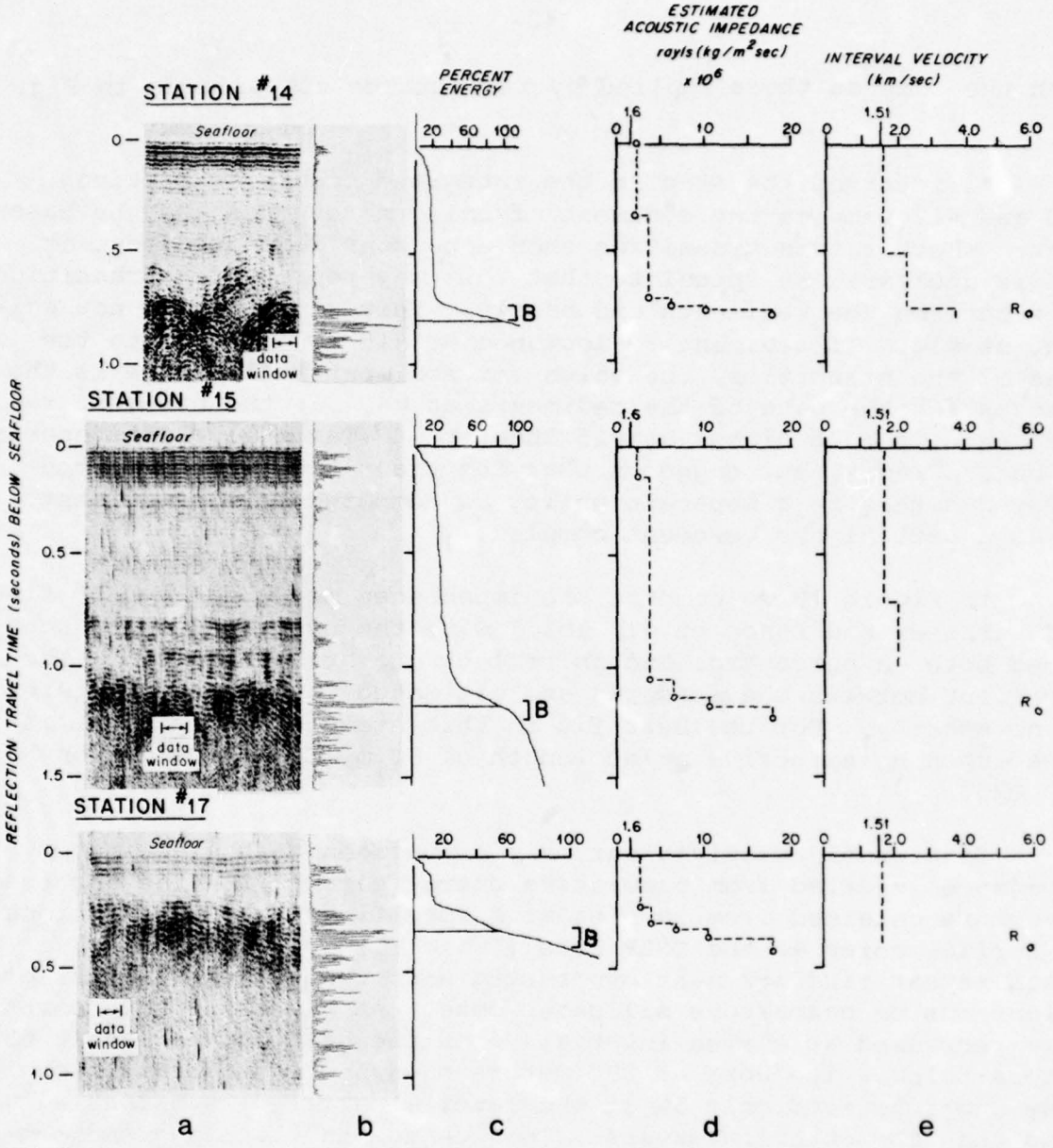

FIG. 14

Stations #14, #15, and #17 - estimated impedance structure with depth; the seismic reflections from which the estimates are derived; and interval velocity.

(a) 3.5 km section of the normal incidence profile at station.

(b) Amplitude-squared trace of one reflection from data window.

(c) Average-shape cumulative energy curve derived from reflection traces of data window, normalized to a standard unit deflection where indicated. Duration of basement return indicated by bracket.

(d) Estimated impedance based on 20-percentile application of model (dashed-line). See Figures 8 and 15.

(e) Interval velocity profile determined at station (o, R = critical refraction velocity determinations).

much the same as those implied by reflectance comparisons in Fig. 12.

An intermediate step in the integrand occurs at stations #15 and #17 between the sediment of uniform response and the basement. Whether this transition should be considered sediment or not is unclear. We speculate that this may represent a transition zone between the sediments and basalt. This structure is not evident at #14. If sediment reflectance at #15 is measured to the base of the transition, the value for sediment reflectance is the same as for the base of the sediments at #4, but the basement reflectance is much higher at #15 than at #4 (Table I). This appears to be a paradox, but suggests that the transition should be considered either as a separate entity as compared to the sediment, or as a part of the basement complex.

In Figure 15 we compare the impedances measured at DSDP site #235 (Fisher and Bunce et al, ibid) with the estimated impedances based both on percentage and on reflectance at station #14. The agreement between the measured and estimated impedance structures is noteworthy. For the best fit in this example, reflectance is based upon an effective pulse length of 80 milliseconds and on α of .029.

Station #14 provides our only comparison of the estimated impedance inferred from cumulative energy curves with the observed structure obtained from samples at a specific site. Descriptions of surface cores at the DSDP site (Table II) obtained from R/V CHAIN repeat findings near other stations, that is, a seafloor of calcareous or calcareous siliceous ooze. At the drill hole cores were recovered at eleven intervals from the seafloor to basalt 650 meters below. The core at 580 meters encountered moderate brown clay and recovered only 3% of the material drilled, substantially less than the other intervals. This change in lithology and competence may be indicative of the transition between sediment and basement seen in the integrands at stations #15 and #17, but such a transition is not apparent at #14.

The report (ibid) gives the acoustic impedance derived from velocity and density measurements. These are not <u>in situ</u> velocity measurements so a value such as 1.47 km/sec for nanno ooze near the seafloor may be less than if measurements were made at the temperature and pressure at depths.

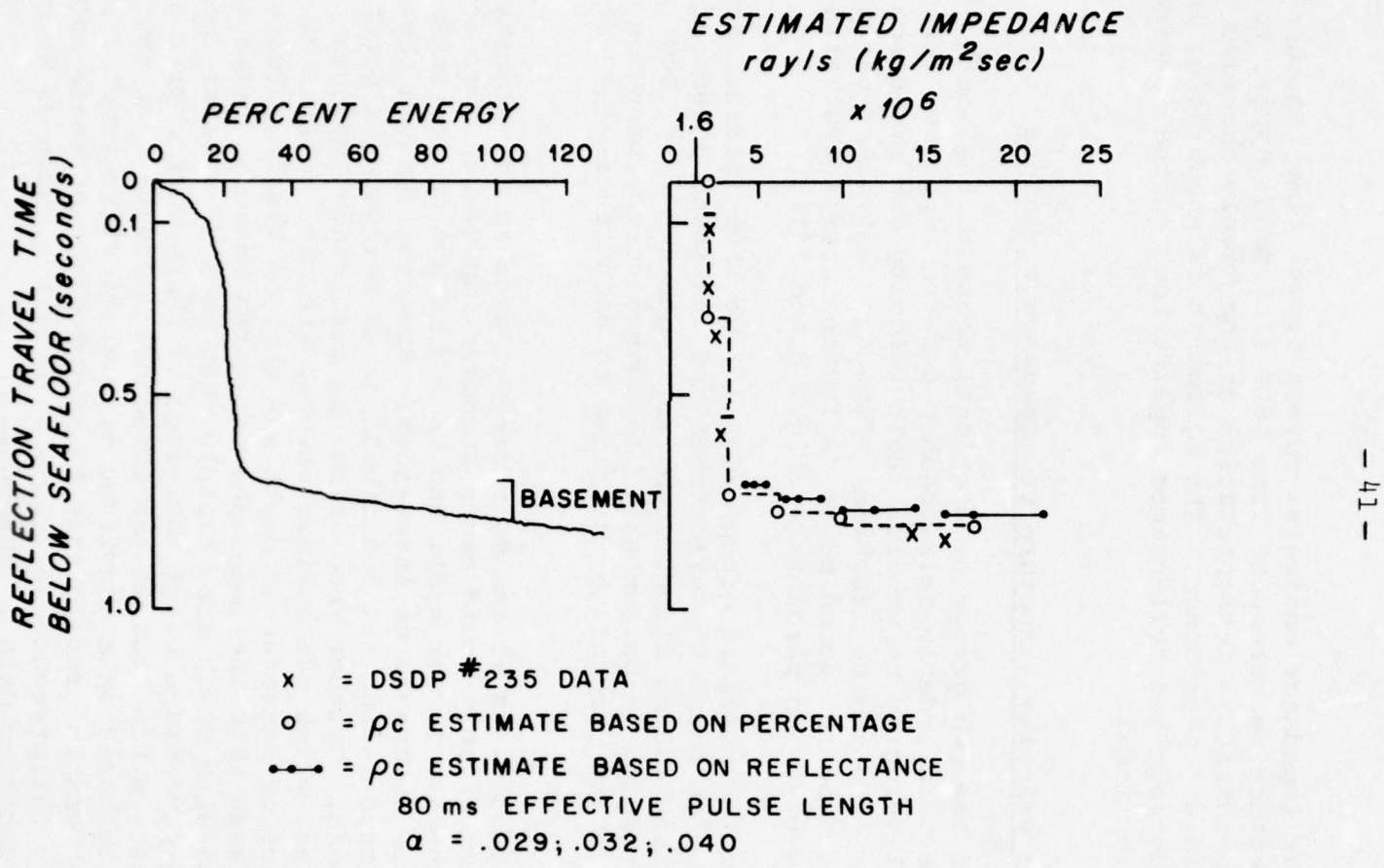

FIG. 15 Station #14. Comparison of DSDP site #235 impedance measurements with impedance estimates based on the 20-percentile and the reflectance applications of the model. Reflectance computed using an 80 millisecond effective pulse length and $\alpha = 0.029$ produces "best" fit.

Our impedance estimates versus travel time together with the impedance measurements from DSDP site #235, appear to confirm the intuitive interpretation of the widely observed "transparent layer" phenomenon. The agreement is encouraging in both the percentage and reflectance applications of the low-frequency reflection model.

Interval velocity structure re impedance structure

Of the two groups of stations, those to the south (Fig. 14) show the more orderly relationship between impedance structure and interval velocity structure. Both velocity and impedance increase together in a logical fashion. Impedance estimates based on reflectance and the sound power reflection coefficient also run close to those based on percentage (Figs. 8 and 15).

In the northern group (Fig. 13) we have included estimates of impedance based on reflectance and the sound power reflection coefficient (50 ms effective pulse length and $\alpha_1 = .040$) as well as those based on percentage. Impedance curves based on reflectance and percentage run close to each other only at station #4.

At stations #3 and #8 there are pronounced velocity inversions, which conceivably would cause stronger impedance inversions, than those at #4. In our model and in our method of determining reflectance we assume no inversions. Squaring removes phase information thus making all contributions to reflectance positive contributions. Further when using the percentage approach the impedance estimates, which are maximum values, are made to fit between the impedance of seawater at depth and that of basalt. Therefore, it can be seen that the impedance estimates based on reflectance would increase with depth more rapidly than both the actual impedance and the percentage based estimates if there were appreciable inversions. Evaluation of the impedance estimate must therefore be partially based on a knowledge of the velocity structure. Conversely when the reflectance based impedance estimate increases too rapidly, the presence of velocity inversions such as we measured in the sonobuoy data is suspected.

Graphic comparisons of reflectance at the stations

Expanded scale integrands of the six stations are compared in terms of reflectance and a common sound power reflection coefficient in Figure 16. Although these comparisons can only be made on an approximate basis because of the uncertainties in pulse length and α , the comparison brings out similarities and differences more clearly than in Figures 13 and 14. The remarkable similarity in the sediment response at station #3 and #4 corroborates what might be expected at adjoining stations. At station #8, compared to #3 or #4, a more gradual rise at the very beginning of the integrand after the onset suggests a change in seafloor character that accounts for the apparent decrease in seafloor reflectivity at #8 (Table I). The similarity of the acoustic stratigraphy in the first 1.25 sec. below seafloor seen on the reflection profiles of stations #3 and #8 (Figure 3a) is less evident in the energetic response. There are a few events during the sediment returns that appear to correlate, but the overall rate of increase of the integrand at #8 is considerably less than at #3 and much closer to that at #14 and #15. This suggests that the transition in impedance structure between #3 and the southern group of stations (Fig. 14) begins to occur at #8 only 150 km southwest of #3.

Contoured traverse profiles

Although our short sections of contoured data show much the same reflectance structure as is found at the respective stations, it is of interest to compare the different contouring methods and to speculate as to continuity or lack of continuity of seabed characteristics along the profiles.

In Figures 9 and 10 (pgs. 26, 27) successive integrands and contours of the integrands along a traverse are presented to examine the continuity of reflectance along the traverse as well as to demonstrate the analysis process. The waveforms shown in Figure 10 are taken from the very beginning of the profile at station #3 shown in Figure 17. Data in Figure 17 are not smoothed to the same extent by the running average algorithm demonstrated in Figure 10, but are otherwise based on the same analysis procedures.

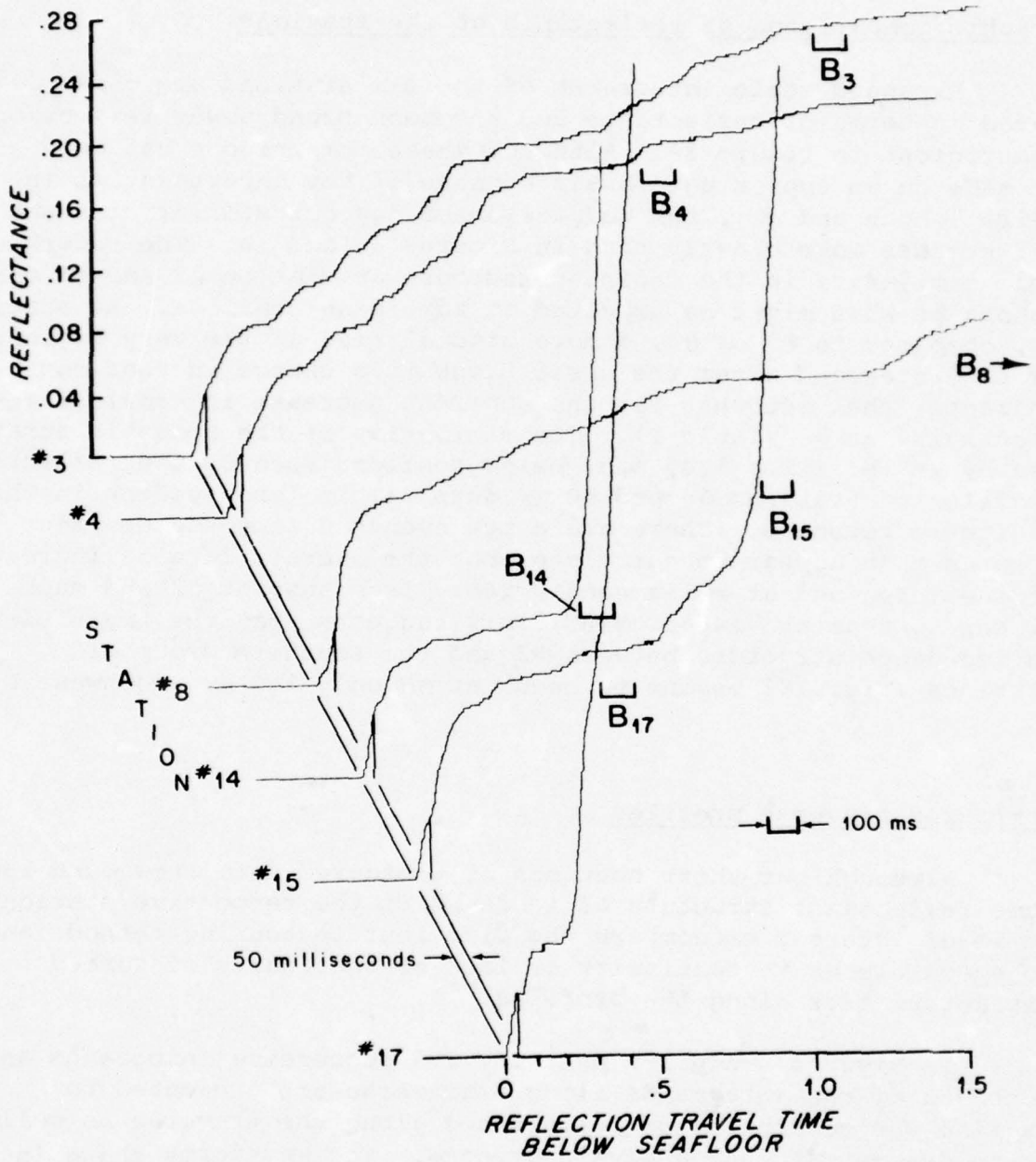

FIG. 16 Comparison of seabed reflectance at the six stations using the average-shape integrand from each station, normalized to a standard unit deflection at 50 milliseconds after onset of returns. Basement returns indicated by brackets.

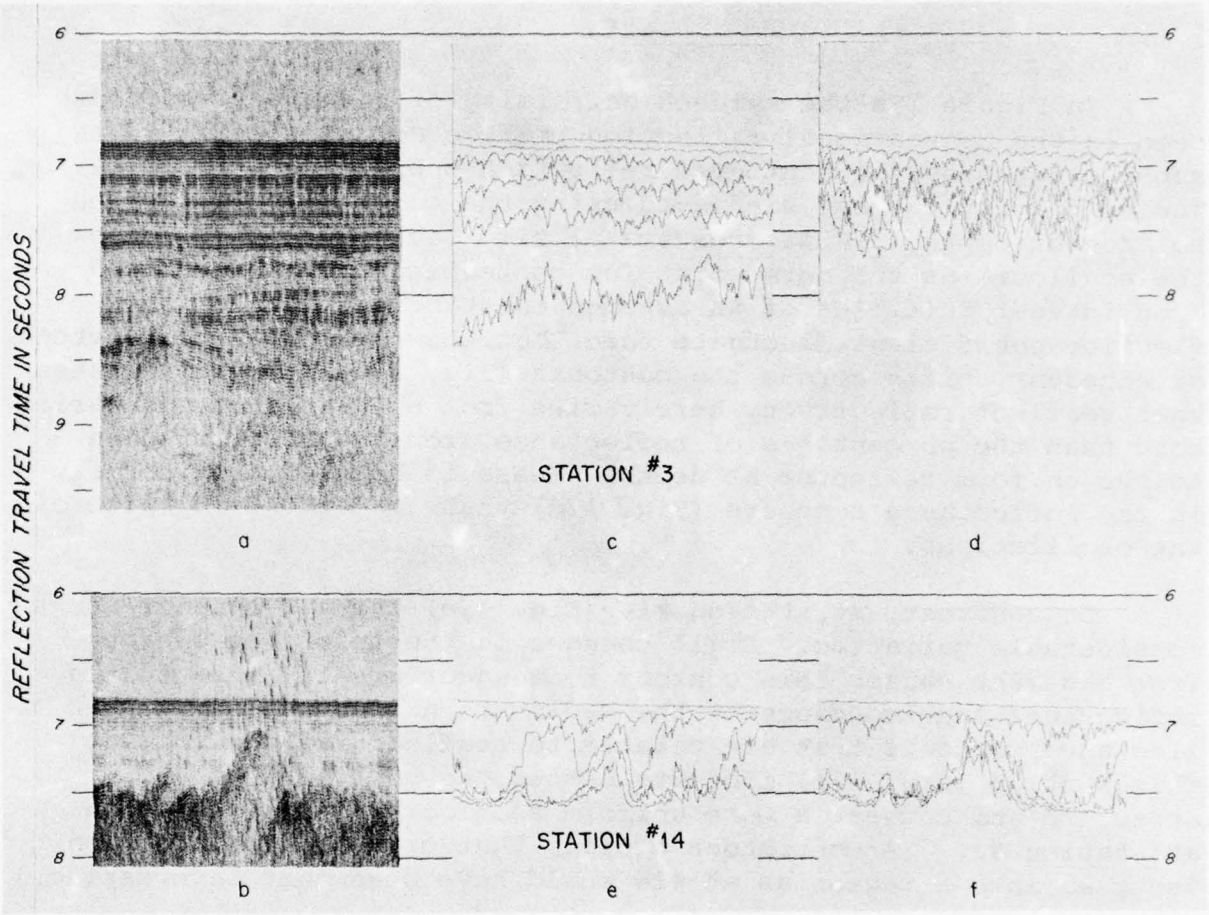

FIG. 17 Seismic reflection profiles at station #3 and #14 with overlays of contoured cumulative energy.

(a) #3 profile crosses a thick (2.3 second) section of sediments; basaltic basement is the rough faint horizon occurring between 8.9 and 9.2 seconds travel time.

(b) #14 profile crosses a thin (0.7 second) section of sediments; basaltic basement is the rough strong horizon occurring at 7.2 to 7.6 seconds travel time.

(c) The reflections occurring between the seafloor reflection at 6.8 seconds and the interface at 7.6 seconds in profile "a" appear to be markedly uniform as in Fig. 10. Normalizing each succeeding cumulative energy curve to a common deflection at 7.6 seconds travel time, the succeeding curves are then contoured to show the travel times of the points on the cumulative energy curve having 0.2, 0.4, 0.6, 0.8, and 1.2 of the unit deflection at 7.6 seconds. Assuming a constant impedance to exist at the interface at 7.5 to 7.6 seconds travel time, these contours serve to show the lateral fluctuations in the impedance of the overlying sediment along the traverse.

(d) The cumulative energy curves can be examined as in Fig. 10 by assuming a uniform reflectivity of the seafloor interface along the traverse and then sectioning the deflection of the cumulative energy curve to determine the travel times at which integer multiplies of the initial deflection occur. Irregularities in travel time indicate there is fluctuation in the initial seafloor return even in areas of uniform sedimentation.

(e) The procedure outlined in "c" is applied to profile "b" using oceanic basement as the reference horizon and using a norm point at 7.6 seconds, about 0.1 second after the start of the basement return.

(f) Using the same procedure in "d", the sediment sequence is shown to be of relatively uniform reflectance and hence, impedance. This inference is clearer here than in profile "e" since this contouring procedure is not affected by the topography in the basaltic basement.

In Figure 17a the evident uniformity of the upper sediments seen in the conventional reflection profile across station #3 is substantiated by the contoured reflection energetics (Fig. 17c). The uniformity is best displayed using the consistent reflection horizon at depth, 7.6 seconds travel time (about 0.8 secs. below the seafloor) as the norm point for contouring. Contours based upon integer multiples of an assumed constant sound power reflection coefficient fluctuate more, but show relatively consistent or coherent shifts across the contours (Fig. 17d). This indicates that seafloor reflectivity here varies from shot-to-shot and varies more than the percentages of reflectance from the seafloor down to the uniform reflector at depth. There is however a uniformity in the reflectance contours (Fig. 17d) that is evident in spite of the oscillations.

In contrast, at station #14 (Fig. 17e) the 40% contour shows considerable variation. Small changes in the reference energy from basement causes this contour to meander greatly because the reflectance and impedance of the sediments are so uniform. Reflectance contours that are related to seafloor reflectivity at this station (Fig. 17f) indicate better the continuity of structure and suggest a more uniform seafloor reflectivity than at station #3. (A continuous profile that crossed from a region as at #3 into a region as at #14 would have been most interesting!)

Mapping characteristics

Too few measurement stations are included in this study to warrant mapping different characteristics. Changes in the different parameters, reflectivity, reflectance, time constants, and Area $_{80}$ would be evident in traverses from one physiographic region to another, but our data here are limited to the relatively short tape recordings taken during the sonobuoy stations.

CONCLUSIONS & RECOMMENDATIONS

1. Our major conclusion is that an "audit" of the seabed reflected energy (reflectance) yields impedance estimates commensurate with the available drilling samples, the compressional wave velocities determined from wide-angle reflection-refraction measurements, the descriptive appearance of the normal-incidence profiling recordings and the seafloor sampling.

2. Two distinct impedance-depth structures are evident in the subject environs of the Somali Basin: (a) A near-linear increase with depth at stations #3, #4 and #8. (b) A non-linear tread-like increase, having a relatively uniform low impedance throughout the sediment column down to a transition zone or to basement at stations #14, #15 and #17. Estimated impedance profiles based on seafloor reflectance show the same trends. The discrepancy between estimates based on percentage and reflectance at stations #3 and #8 can be explained by accounting for the presence of impedance inversions by the pronounced interval velocity inversions measured at the stations. Otherwise differences are probably the result of uncertainties in seafloor reflectivity and pulse length. Agreement between impedance estimates based on percentage and reflectance is quite acceptable when these two parameters are adjusted to the pulse length and sound power reflection coefficient measured at 30 to 60 Hz.

3. Seafloor reflectivity in the 30-60 Hz passband is quite uniform at the six stations, median 0.19, but the subtle differences observed appear to be the key to agreement between the percentage and reflectance based estimate of impedance. When examined over a wider range of frequencies, the reflectivity shows more variability, from 0.12 to 0.30. Seafloor cores consist primarily of calcareous-siliceous ooze, suggesting uniformity in seafloor composition as well as reflectivity.

4. Since reasonable agreement is obtained between the cored results at DSDP #235 and the estimates of acoustic impedance, it appears that the assumptions re internal reflection multiples, plane wave propagation, absorption and scattering are practical assumptions to make when working at low frequencies such as the 30 to 60 Hz passband.

5. We conclude that there is need for further application of this type of analysis and that measurements of reflectivity, reflectance and impedance estimates are of unique utility in interpretation of seismic reflection profiles. The application of the analysis will be of specific interest:

a. to provide better assessment of the characteristics and the continuity of the characteristics of the seabed for implanting materials, instruments and drilling. This type of assessment is germane to better correlation between the acoustic record and the characteristics of cored sediments and to an improved evaluation of the lateral homogeneity of materials between core or drill holes.

b. to examine within the transitional phenomena along profiles the manner in which seafloor reflectivity relates to changes in grain size and sorting, and in differentiation between pelagic, turbidity, and contourite deposits. This requires more resolution than available in this study but could be accomplished by using higher frequencies, i.e. sound pulses with center frequencies at 3.5 and 12 kHz. It is relatively straight forward to include estimates of transmission, absorption and scattering losses at the higher frequencies.

c. to provide additional information with which to evaluate determinations of interval velocities from wide angle reflection-refraction profiles, from sonobuoys or multi-channel arrays. The reflectivity of the seafloor restricts the range of velocities of the first layer, and the reflectance, the impedance of the deepest observed reflection. Should the impedance estimates increase to an impedance value such as that of basalt at a travel time earlier than observed, the presence of velocity and/or impedance inversions is suggested.

d. to make quantitative measurements of the shot-by-shot reflection variability, to examine and possibly to identify the mechanisms producing this variability, and to use the variability as a measure of seafloor and seabed character.

ACKNOWLEDGMENTS

The completion of this study has been supported by the Office of Naval Research (ONR), Contract N00014-74-C0262, NR 083-004 and a grant from the Ocean Industry Program of the Woods Hole Oceanographic Institution; initial phases were supported under National Science Foundation Grant (NSF) GA-27516 and ONR N00014-66-C0241, NR 083-004.

S. T. Knott and Hartley Hoskins evolved this approach in an effort to utilize the amplitude information in seismic profiling. E. O. LaCasce, Jr., did the mathematical analysis, contributing his time while on sabbatic leave from the Physics Department of Bowdoin College during the 1975-76 academic year. One of his students, Douglas D'Ewart, contributed his two-week spring leave to data reduction. The digital seismic analysis system, procured largely by IDOE-NSF grant 28193, was made available by K. E. Prada. His flexible system and personal assistance made possible our manipulation and display of data. Aileen W. Poehls assisted in preliminary examinations of data and program developments. Suzanne Dynan carried out programming changes for the many phases of data analysis as we reduced trials to systematic practice, reduced data,prepared material for figures and helped edit text. Shirley Waskilewicz prepared the typescript and Ruth Davis the figures. E. T. Bunce, J. I. Ewing, and G. M. Purdy kindly reviewed the text.

REFERENCES

Baggeroer, Arthur B., and Hartley Hoskins, 1975, "Seismic Filter Design Using Scattering Function Theory and Source Monitor Signals" Woods Hole Oceanographic Institution Ref. No. 74-69, 55p.

Baggeroer, Arthur B., Knott, S.T., Hoskins, H. and Bunce, E.T., 1973, "Digital Signal Processing of Oceanic Seismic Profiler Data" 1972. Reflectivity and sediment Classification, Woods Hole Oceanographic Institution Ref. No. 73-38, 11p.

Baxter, Lincoln, II, 1958 "Development of Sound Analysis Equipment for Sonar Research" Part I, Woods Hole Oceanographic Institution Ref. No. 58-12, 12p; 1960, Part II, Woods Hole Oceanographic Institution Ref. No. 60-25, 7p.

Borcherdt, Roger D., 1973. "Energy and Plane Waves in Linear Visco-elastic Media" Jour. Geophy. Res. Vol. 78, No. 14, p. 2442-2453.

Breslau, L., 1966. "Classification of Sea-Floor Sediments with a Shipborne Acoustical System" LePetrole et la Mer Sec 1 No. 132, 9p.

Bunce, Elizabeth T. and J. B. Hersey, 1966, "Continuous Seismic Profiles of the Outer Ridge and Nares Basin North of Puerto Rico" Geol. Soc. Am. Bull. Vol. 77, No. 8, p. 803-812.

Claerbout, Jon F., 1968. "Synthesis of a Layered Medium from its Acoustic Transmission Response" Geophysics, Vol. 33, No. 2, p. 264-269.

Emery, K. O. and Elazar Uchupi, 1965. "Structure of Georges Bank" Marine Geology, Vol. 3, p. 349-358.

Ewing, J. I., 1963. "Elementary Theory of Seismic Reflection and Refraction Measurements" Chap. 1 in Vol. 3 of the Sea: Ideas and Observations in the Study of the Sea, M. N. Hill, Ed., Interscience-Wiley, 963 p, p. 3-19.

Ewing, J. and M. Ewing, 1962. "Reflection Profiling in and around the Puerto Rico Trench" Jour. Geophy. Res. Vol. 67, #12, P. 4729-4739.

Ewing, John I., J. Lamar Worzel and Maurice Ewing, 1962. "Sediments and Oceanic History of the Gulf of Mexico", Jour. Geophy. Res. Vo. 67, No. 6, pp. 3509-3527.

Ewing, Maurice, John I. Ewing, and Manik Talwani, 1964. "Sediment Distribution in the Oceans: The Mid-Atlantic Ridge" Geol. Soc. Am. Bull. Vol. 75, No. 1, p. 17-36.

Fisher, R. L., E. T. Bunce, et al, 1974, "Initial Reports of the Deep Sea Drilling Project" Vol. XXIV, U. S. Govt. Printing Office, 1183 p.

Fowles, Grant R, 1975. "Introduction to Modern Optics, Second Edition" Holt, Rinehart and Winston, 328 p.

Gupta, Ravindra N, 1965. "Reflection of Sound Waves from Transition Layers" Jour. Acoustical Soc. Am. Vol. 39, No. 2, p. 255-260.

Hamilton, Edwin L., 1970. "Prediction of In-situ Acoustic and Elastic Properties of Marine Sediments" Geophysics, Vol. 36, No. 2, pp. 266-284.

Hamilton, Edwin, 1971. "Elastic Properties of Marine Sediments" Jour. Geophy. Res. Vol. 76, No. 2, p. 579-604.

Hamilton, Edwin L., 1976. "Sound Attenuation as a function of Depth in the Sea Floor" Jour. Acoust. Soc. Am. Vol. 59, No. 3., p. 528-535.

Hermont, A. J., 1969. "Is Seismic Energy of Diagnostic Value?" Geophysics, Vol. 34, No. 2, p. 196-212.

Hersey, J. B., 1963. "Continuous Seismic Profiling" Chap. 4 in Vol. 3 of "The Sea: Ideas and Observations in the Study of the Sea" M. N. Hill, Ed., Interscience-Wiley, 963 p. pp 47-72.

Hersey, J. B. and M. Ewing, 1949. "Seismic Reflectors from Beneath the Ocean Floor" Trans. Am. Geophy. Union. Vol. 30, p. 5-14.

Houtz, Robert E., John Ewing and Xavier LePichon, 1968. "Velocity of Deep-Sea Sediments from Sonobuoy Data" Jour. Geophy. Res. Vol. 73, No. 8, p. 2615-2641.

Kinsler, L. E. and A. R. Frey, 1962. "Fundamentals of Acoustics" 2nd Ed. John Wiley and Sons, New York 524 p.

Knott, C. G. 1899. "Reflexion and Refraction of Elastic Waves, with Seismological Applications in Philosophical Mag., S. 5, Vol. 48, No. 290, p. 64-97.

Knott, S. T. and H. Hoskins, 1968. "Evidence of Pleistocene Events in the Structure of the Continental Shelf off the Northeastern United States" Marine Geology, Vol. 6, p. 5-43.

Knott, S. T., Hartley Hoskins, A. B. Baggeroer, and E. T. Bunce, 1972. "Digital Signal Processing of Oceanic Seismic Profiles Data, 1971" Woods Hole Oceanographic Institution Ref. No. 72-69, 17 p.

Moore, David G. and Joseph R. Curray, 1963. "Sedimentary Framework of the Continental Terrace Off Norfolk, Virginia and Newport, Rhode Island" Bull. A.A.P.G., Vol. 47, No. 12, p. 2051-2054.

Nafe, John E., 1957. "Reflection and Transmission Coefficients at a Solid-Solid Interface of High Impedance Contrast", Bull. Seis. Soc. Am. Vol. 47, No. 3, p. 205-219.

Nafe, John E. and Charles L. Drake, 1957. "Variation with Depth in Shallow and Deep Water Marine Sediments of Porosity, Density, and the Velocities of Compressional and Shear Waves" Geophysics, Vol. 22, No. 3, p. 523-552.

Officer, C. B., 1955. "A Deep-Sea Seismic Reflection Profile" Geophysics, Vol. 20, p. 270-282.

Prada, K. E., 1976. "System Overview, Developmental History, Design and Implementation" Vol. 1 of "WHOI/IDOE Digital Seismic Data Acquisition and Analysis System", Woods Hole Oceanographic Institution Ref. No. 76-38.

Rona, Peter A. and C. S. Clay, 1967. "Stratigraphy and Structure along a Continuous Seismic Reflection Profile from Cape Hatteras, North Carolina to the Bermuda Rise" Jour. Geophy. Res. Vol. 72, p. 2107-2130.

Shor, G. G., Jr., 1959. "Reflexion Studies in the Eastern Equatorial Pacific" Deep-Sea Research, Vol. 5, p. 283-289.

Talwani, Manik and Olav Edlholm, 1972. "Continental Margin off Norway: A geophysical study", Geol. Soc. Am. Bull. Vol. 83, p. 3575-3606.

Tyce, Robert C., 1976. "Near-bottom Observations of a 4 kHz Acoustic Reflectivity and Attenuation" Geophysics, Vol. 41, No. 4, p.

Whitmarsh, R. B., 1972, "Discussion and Interpretation of Some Physical Properties", Chap. 12 in A.S. Laughton, W. A. Baggren, et al., Initial Reports of the Deep Sea Drilling Project, Vol. XII, pp. 935-951.

Wolf, Alfred, 1937. "The Reflection of Elastic Waves from Transition Layers of Variable Velocity" Geophysics, Vol. 2, No. 4, p. 357-363.

Appendix I Reflectance of a seabed consisting of two layers.

A simplified representation of ray paths for seismic profiling is shown in Figure I-1. An intermediate layer of material with a characteristic impedance, $\rho_1 c_1$, is between the water ($\rho_0 c_0$) and the acoustic basement material ($\rho_2 c_2$). A continuous acoustic wave with an initial amplitude, B_0 strikes the first interface at normal incidence. (For clarity the figure is drawn with the rays at an angle.) At the first interface part of the beam is transmitted and part reflected. The transmitted beam encounters the second interface where it is partly reflected and partly transmitted. The reflected beam returns to the first interface where again reflection and transmission occur. This process continues with an infinite number of reflections and a steady-state situation is obtained.

At the first interface the reflection coefficient from water to the intermediate layer is

$$r_{01} = \frac{\rho_1 c_1 - \rho_0 c_0}{\rho_1 c_1 + \rho_0 c_0} = \frac{z_1 - 1}{z_1 + 1} \qquad \text{Eq. I-1}$$

where Z_1 is the ratio of the acoustic impedances, $\rho_1 c_1 / \rho_0 c_0$. For a reflection at this interface within the layer, the reflection coefficient r_{10} is equal to ($-r_{01}$). The transmission coefficient across the first interface from the water to the intermediate layer is

$$t_{01} = \frac{2 \rho_1 c_1}{\rho_0 c_0 + \rho_1 c_1} = \frac{2 z_1}{z_1 + 1} \qquad \text{Eq. I-2}$$

But the transmission coefficient across the first interface from the layer to the water is

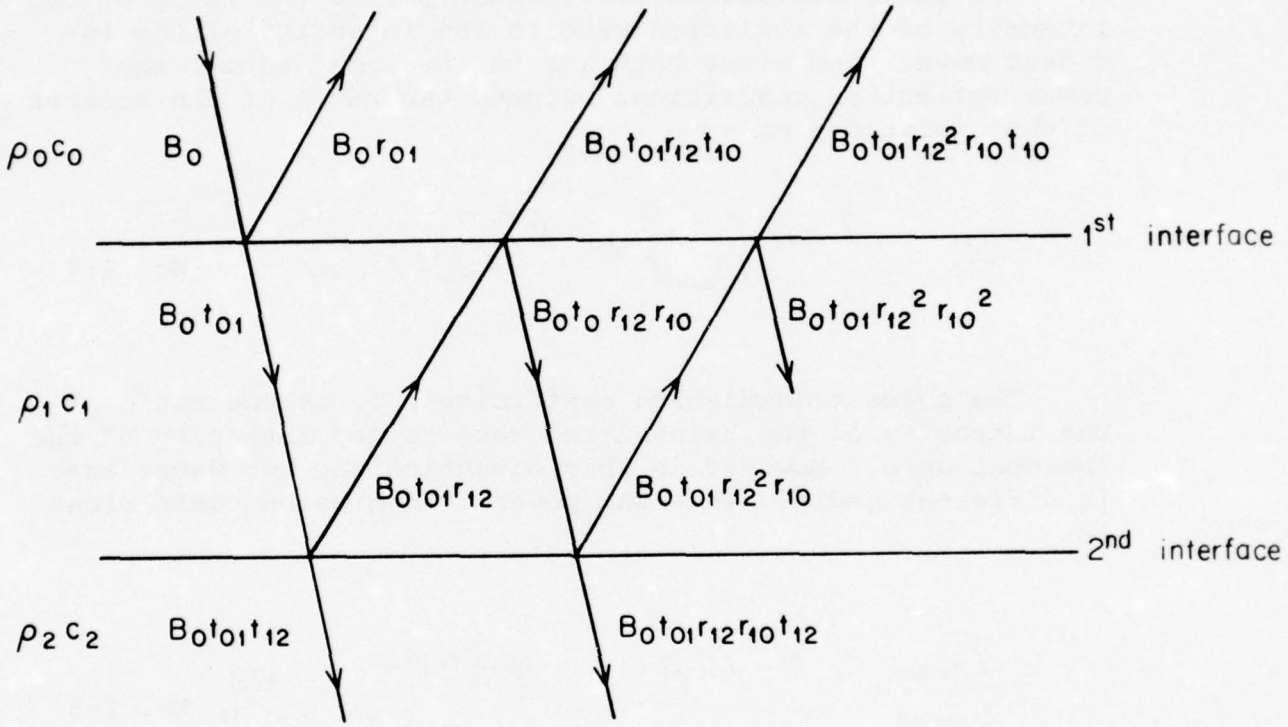

FIG. I-1 A schematic diagram of the transmission paths of a wavefront at normal incidence on a two layer seabed. (For clarity, the rays are drawn at an angle.)

$$t_{10} = \frac{2\rho_0 C_0}{\rho_0 C_0 + \rho_1 C_1} \qquad \text{Eq. I-3}$$

The power reflection coefficient, α, is the ratio of the intensity of the reflected wave to the intensity of the incident wave. And since both are in the same medium, the power reflection coefficient becomes the ratio of the squares of the amplitudes or

$$\alpha_1 = I_{refl} / I_{incid} = B_1^2 / B_0^2 = r_{01}^2 \qquad \text{Eq. I-4}$$

The power transmission coefficient, T, is the ratio of the intensity of the transmitted wave to the intensity of the incident wave. However in this situation the two waves are in different media. Thus the power transmission coefficient is

$$T = \frac{I_{trans}}{I_{incid}} = \frac{B_1^2 / 2\rho_1 C_1}{B_0^2 / 2\rho_0 C_0} = \frac{4\rho_0 C_0 \rho_1 C_1}{(\rho_0 C_0 + \rho_1 C_1)^2} = \frac{4Z_1}{(Z_1+1)^2} \qquad \text{Eq. I-5}$$

Notice that T_1 is equal to the product of t_{01}, and t_{10} and that $\alpha_1 + T_1 = 1$.

In the more common situation the intensity of the transmitted waves is computed, but for seismic profiling the observed quantity is the reflected waves. Although the instantaneous amplitude is recorded, the energy (intensity) is the quantity that is used in the analysis. According to the Principle of Superposition, the amplitudes of the reflected components must be added with their proper phase.

Then the intensity is computed from the resultant amplitude.

The phase change due to reflection at an interface is assumed to be 0 or 180 degrees. The phase change, δ, due to the path difference is (path difference/wave length) or $(2\,k\,h)$, where h is the thickness of the layer. (Note that in computing the intensities, phase changes of 180° will not effect the results.)

In Figure I-1 the amplitudes of the waves are given after each reflection or transmission, thus the amplitude of the first reflected wave B_0 is $B_0 r_{01}$ and the first transmitted wave, $B_0 t_{01}$. The order of the subscripts is related to the direction of wave at each event. The phase changes are not included in this figure.

The component that enters the layer is reflected from the second interface, and finally it re-enters the water. So its amplitude is $B_0 t_{01} r_{12} t_{10}$. The resultant amplitude including the phase difference between successive waves can be written as

$$B_{refl} = B_o r_{01} + B_o t_{01} r_{12} t_{10} e^{j\delta} + B_o t_{01} r_{12}^2 r_{10} t_{10} e^{j2\delta} + \cdots$$

The common terms may be factored from the infinite series so

$$B_{refl} = B_o \left\{ r_{01} + \frac{t_{01} t_{10}}{r_{10}} \left[r_{12} r_{10} e^{j\delta} + \left(r_{12} r_{10} e^{j\delta} \right)^2 + \cdots \right] \right\}$$

But $t_{01} t_{10} = T_1$. Also the series in the brackets is a geometric progression with a ratio $(r_{12} r_{10} e^{\;})$, and thus it is readily summed. The reflected amplitude may thus be written as

$$B_{refl} = B_o \left[r_{01} + \frac{T_1 r_{12} e^{j\delta}}{1 - r_{12} r_{10} e^{j\delta}} \right]$$

This equation may be simplified if all quantities are over the common denominator. In the algebraic rearrangement, the

identities $T_1 = 1 - r_{10}^2$ and $r_{01} = -r_{10}$ are used. The equation may then be written as

$$B_{refl} = B_o \left[\frac{r_{01} - r_{12} e^{j\delta}}{1 - r_{12} r_{10} e^{j\delta}} \right]$$

The resultant amplitude is a complex quantity. Thus the intensity is the product of the resultant amplitude and its complex conjugate. By using the Euler Relation the reflected intensity becomes

$$I_{refl} = I_0 \left[\frac{r_{01}^2 + r_{12}^2 - 2 r_{10} r_{12} \cos\delta}{1 + r_{12}^2 r_{10}^2 - 2 r_{10} r_{12} \cos\delta} \right]$$

Or in terms of the power reflection coefficients

$$I_{refl/I_0} = \frac{\alpha_1 + \alpha_2 - 2\sqrt{\alpha_1 \alpha_2} \cos\delta}{1 + \alpha_1 \alpha_2 - 2\sqrt{\alpha_1 \alpha_2} \cos\delta} \qquad \text{Eq. I-6}$$

which is what we have termed the reflectance, $\mathcal{R}$, for the single layered seabed with two interfaces.

Appendix II Comparison of the reflectance computations for a two layer seabed as a function of ρ, c_1

The equation for the reflectance derived in Appendix I is for a steady state wave with a single frequency. The signals used in seismic profiling are broadband pulses. The electronic processing of the received signal permits the analysis to be done in a smaller band of frequencies but not on a single frequency. Also the computational problems involved in using Eq. I-6 can be reduced by the use of an approximation for a broader band signal. The reduced form for the reflectance from a single layer with two interfaces is given by Eq. 3.

$$R_2 = \alpha_1 + T_1^2 \alpha_2 \qquad \text{Eq. II-1}$$

The range of acoustic impedances commonly encountered in deep sea seismic profiling is from water to basalt or a ratio with respect to water of about 1 to 10. By picking values of ρc between water and basalt the reflectance can be computed by Eq. II-1 and by Eq. I-6. However in the case of Eq. I-6 the effective path difference must be included. So for the response due to a relatively broadband signal we will compute the reflectance by Eq. I-6 for path differences between 0° and 180° in steps of 20°. Then we will take the average for comparison purposes.

Table II-1 gives the results of these computations. Here $Z_1 = \rho_1 c_1 / \rho_0 c_0$ is the relative acoustic impedance between the layer and water. By letting Z_1 vary between 1 and 10, the effect is to consider the layer between the water and the basalt to vary in acoustic impedance from water to basalt.

Table II-1

Reflectance

Z_1	Eq. II-1	Eq. I-6
1	.67	.67
2	.46	.47
4	.44	.43
6	.53	.52
8	.61	.60
10	.67	.67

The differences shown in this table are relatively small, certainly within the experimental error entailed in the measurements.

Appendix III A simplified derivation for the reflectance from a many layered seabed.

In Appendix I the reflectance from a seabed with one layer and two interfaces is analyzed. This analysis sums the amplitudes of all of the multiple reflections with the proper phase included. The relative intensity is then obtained from the square of the relative amplitude.

In Appendix II we show that the relative intensity as computed from the average over the acoustic wavelengths for a broad band signal is approximately the same as the relative intensity obtained by neglecting the phase relations between successive reflections. In the situation most commonly encountered in the seabed, the successive layers tend to be compressed with depth producing increasing values of acoustic impedance. In other words, the power reflection coefficient between the individual layers is small and the transmissivity is large.

These two conditions, averaging of the phases and the small power reflection coefficient between layers, permits a simplified derivation for the reflectance for a multi-layered seabed. Since we are not considering the phase relations, we may deal directly with the intensities. And since the power reflection coefficient is small we need to consider only the first reflection from each surface. With these conditions, the reflection process is indeed that shown in Figure III-1. (Note that the incoming and reflected signals are at normal incidence but they are drawn at an angle to clarify the process). The intensity of the incoming signal is I_0. At the first interface, it is partly reflected ($\alpha_1 I_0$) and partly transmitted ($T_1 I_0$). When the transmitted signal encounters the second interface, partial reflection ($T_1 \alpha_2 I_0$) and partial transmission ($T_1 T_2 I_0$) occurs. The upgoing signal returns to the first interface where the transmitted portion ($T_1^2 \alpha_2 I_0$) is the part that returns to the receivers on the surface. The process continues at the successive surfaces as shown in the diagram.

To show that the second reflection term is much smaller

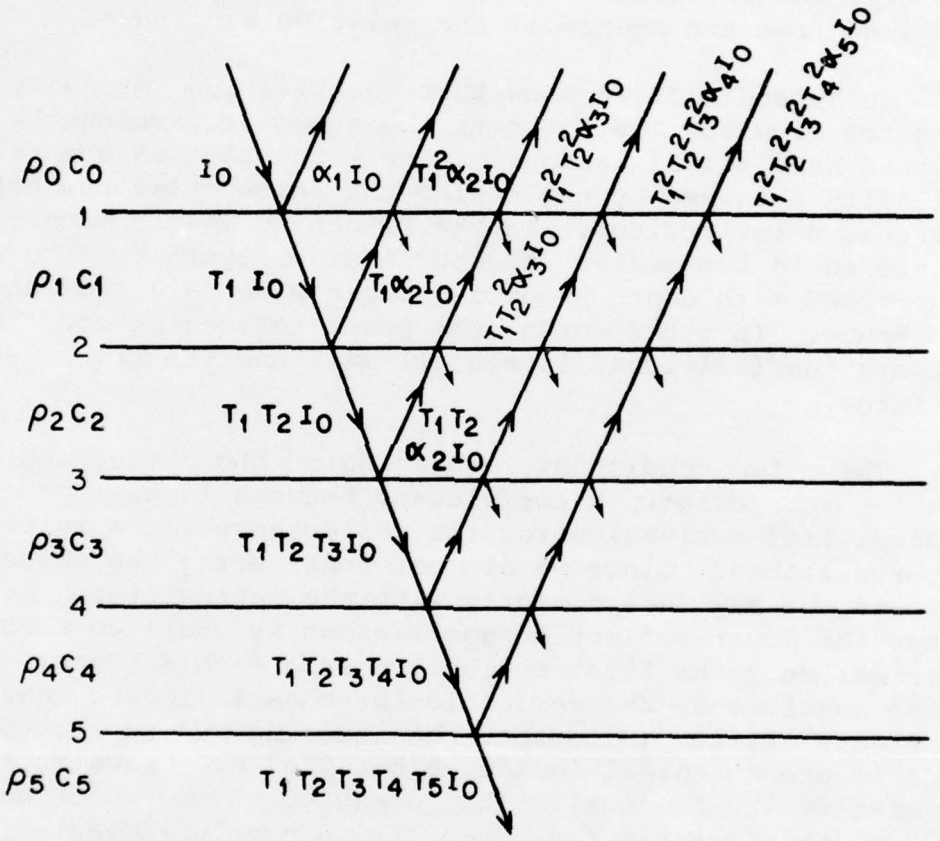

FIG. III-1 A schematic diagram to show the reflection of a pulse from a layered seabed. (The incoming pulse is at normal incidence. The figure is drawn at an angle to clarify the reflection paths).

and that it may be negligible for the accuracy of our measurements, we will compare the magnitude of the first and second reflections from the first interface. The intensity of the first reflection is, as described above, $(T_1^2\ \alpha_2\ I_0)$. For the signal that is reflected the second time from the second interface before returning to the receiver, the intensity is $(T_1^2 \alpha_2^2 \alpha_1 I_0)$ or $(\alpha_1 \alpha_2)$ times smaller than the first reflection. With α_1 and α_2 on the order of one-tenth, their product is on the order of one-hundredth or negligibly small.

Thus the signal returned to the receiver from a specific interface is the product of the square of the power transmission coefficients for the intervening interfaces and the power reflection coefficient for that interface. These return signals are shown for a four layered seabed with five interfaces in Figure III-1. Since the reflectance for the seafloor is the ratio of the net reflected signal to the incident signal, the reflectance is readily calculated as:

$$R_5 = \alpha_1 + T_1^2\alpha_2 + T_1^2T_2^2\alpha_3 + T_1^2T_2^2T_3^2\alpha_4 + T_1^2T_2^2T_3^2T_4^2\alpha_5$$

Eq. III-1

which is the same as Eq. 4.

In Figure III-2 the reflectance for the received signal for three types of seabeds is plotted. These reflectances are computed from Eq. III-1 and are mathematical models. They are not intended as an attempt to model data; rather these figures are intended to show the effects of different acoustic impedances for the successive layers. The first curve is the result of equal increments in the relative acoustic impedances between water and basalt. In the second curve, the effect of a strong reflector at the second interface is shown. For the third curve the interfaces reflect approximately equal energies.

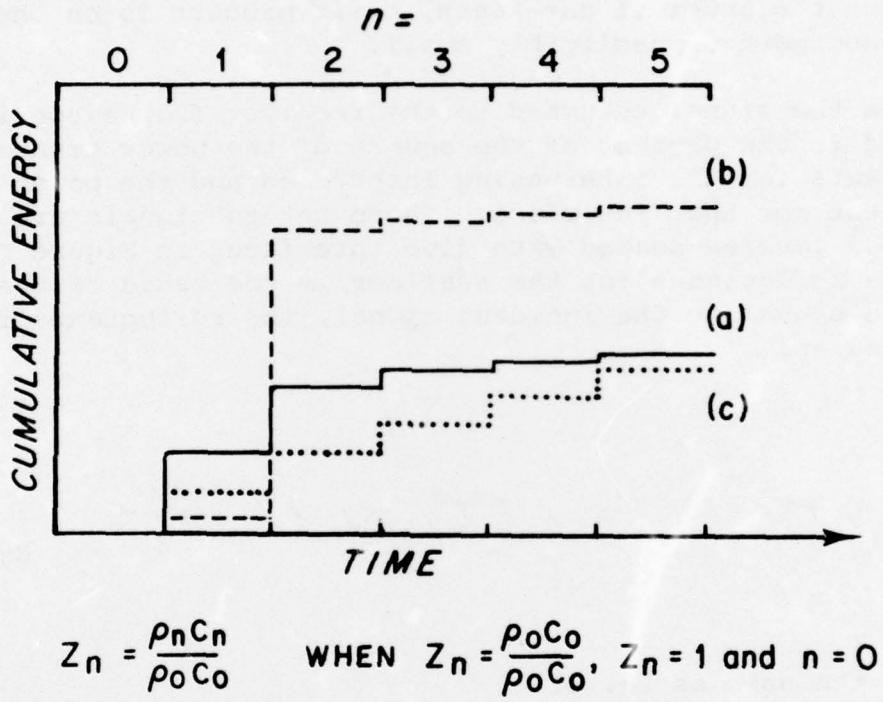

FIG. III-2 Computed energy integrands for selected relative impedances of the seafloor.

(a) Equal increments in the relative acoustic impedances between water and basalt Z_n = 1, 2, 4, 6, 8, 10.

(b) The effect of a strong reflector at the second interface Z_n = 1, 1.3, 6, 7.5, 8.5, 10.

(c) For interfaces that reflect approximately equal energies Z_n = 1, 1.5, 2.4, 3.7, 6.0, 10.

Appendix IV. Gradation of seabed acoustic impedance with depth re reflectance.

The relationship of the magnitude of reflectance at various travel times on the integrand to the magnitude of the return from a reference horizon such as basaltic basement gives an indication of the impedance characteristics with depth. Figure IV-1 indicates the reflectance from a sequence of interfaces between synthetic layers, each of which produces an equal reflected energy increment. The maximum reflectance is constrained by an upper limit of impedance, that of basalt. If the seafloor were basalt, the Rayleigh reflection coefficient would be approximately 0.83 and about 69% of the incident energy would be reflected back into the water, using acoustic impedances of 1.6×10^6 kg/m^2 sec for sea water and 18×10^6 for basalt.

This is apparent in Figure IV-1 when entering the graph at the appropriate reflectivity. One interface is involved and it is characterized by a high impedance contrast. As more intervening layers are introduced between the seawater and basalt, each having appropriate impedances to fit the equal energy step model, the reflectance in relation to basaltic basement decreases. Neglecting transmission losses, absorption and scattering, the total amount of energy reflected back into the water is reduced and the amount of energy transmitted into the basalt presumably increases.

This same effect may also be examined by plotting the reflectance of a three-layer geological model (sea-water, intermediate-layer, basalt) in which the impedance of the intermediate layer varies from that of seawater to that of basalt (Fig. IV-2).

Carrying this examination one step further to a four layer model bounded by seawater and basalt with two intermediate layers, an approximate plot of "total" reflectance contours computed relative to the basaltic basement return shows the effects of an impedance inversion (Fig. IV-3). If the impedance of the third layer is low relative to that of basalt as well as that of the overlying layer (an impedance inversion within the intermediate

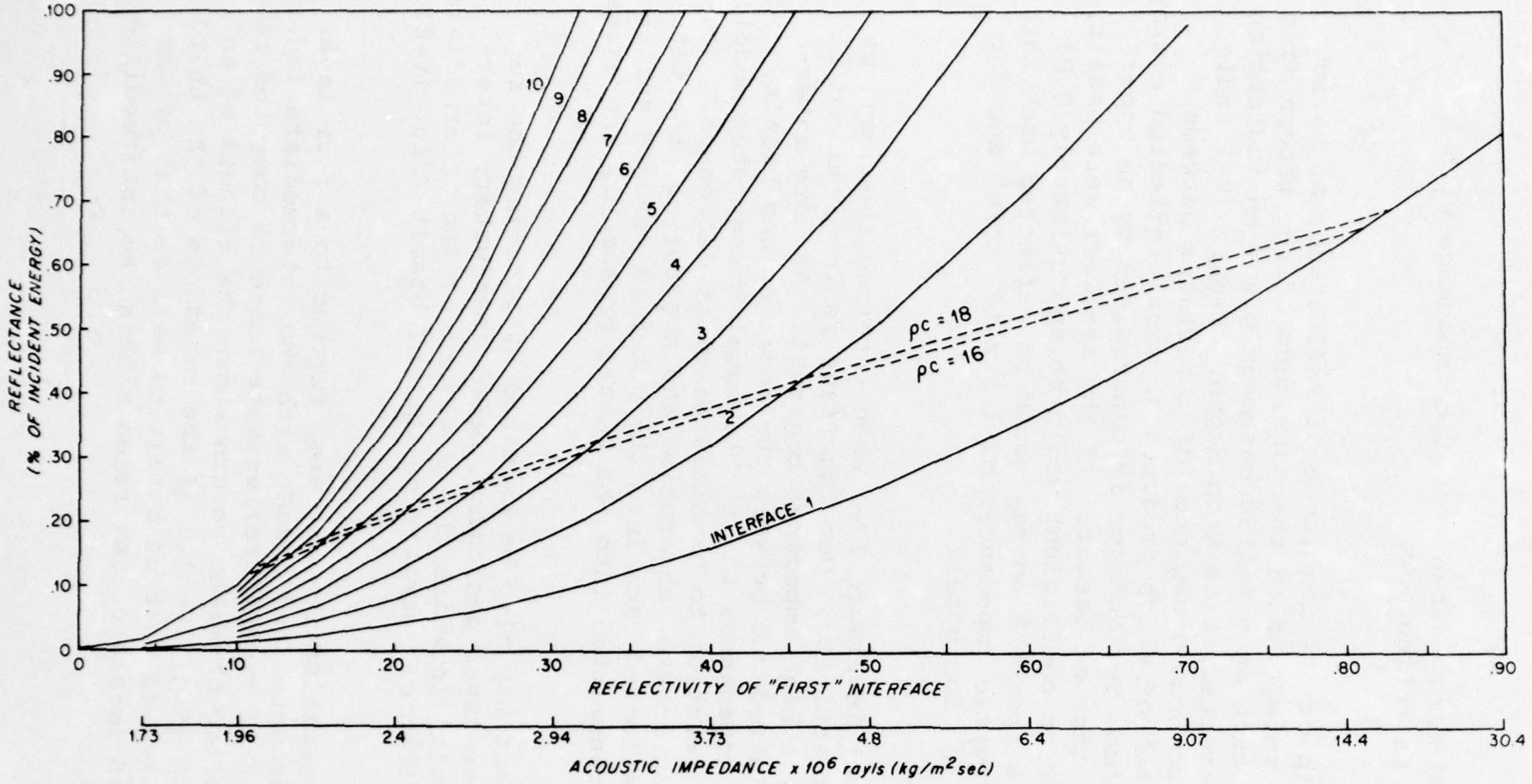

FIG. IV-1 Plot of the reflectance of the sequence of "layers" of increasing impedance shown in Fig. 7. Each "layer" produces an equal increment on the cumulative energy curve.

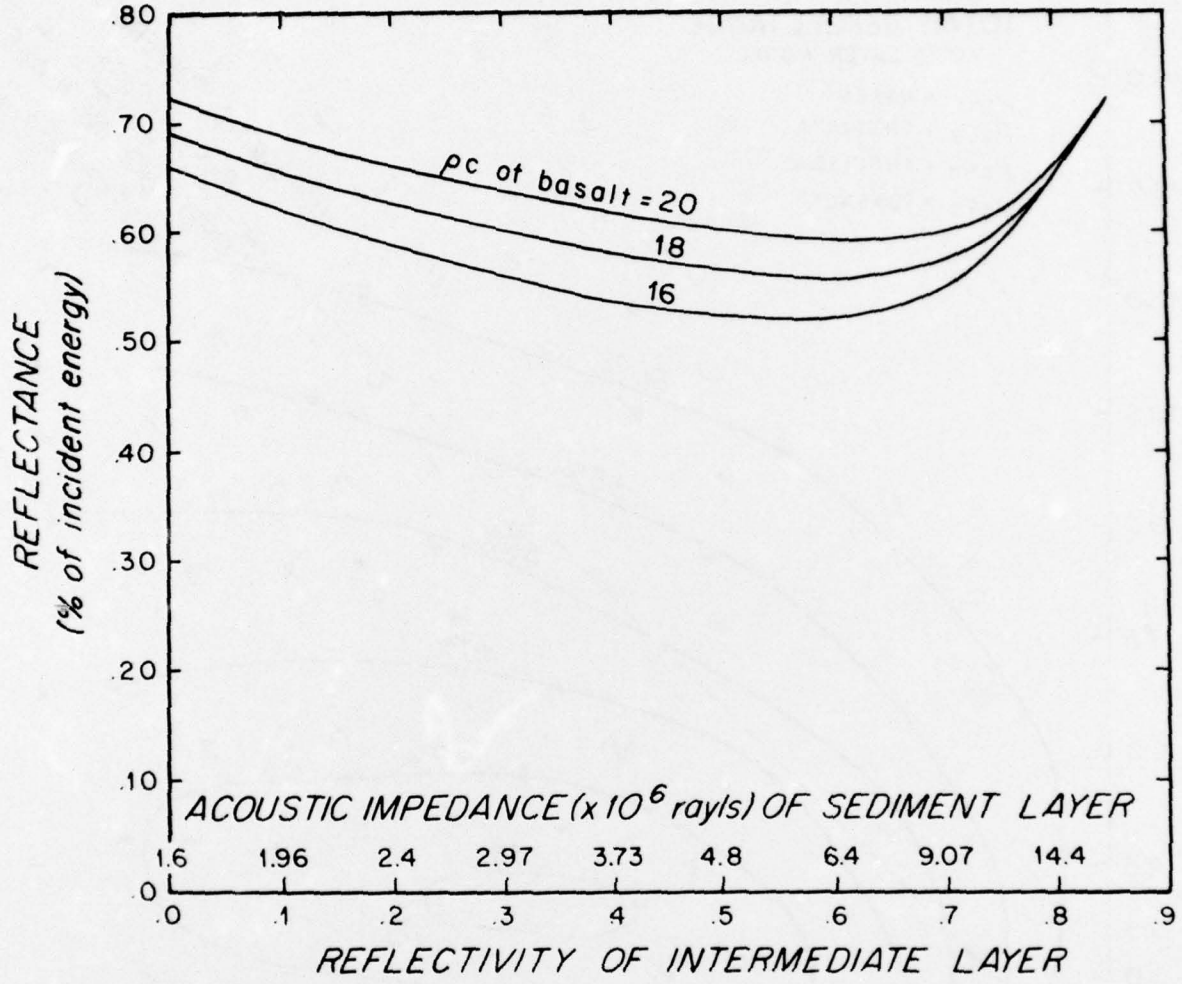

FIG. IV-2 Plot showing change in reflectance as a function of the impedance of one intermediate layer. Total amount of energy reflected back into the water is reduced when we introduce a layer of intermediate impedance between the water and basalt.

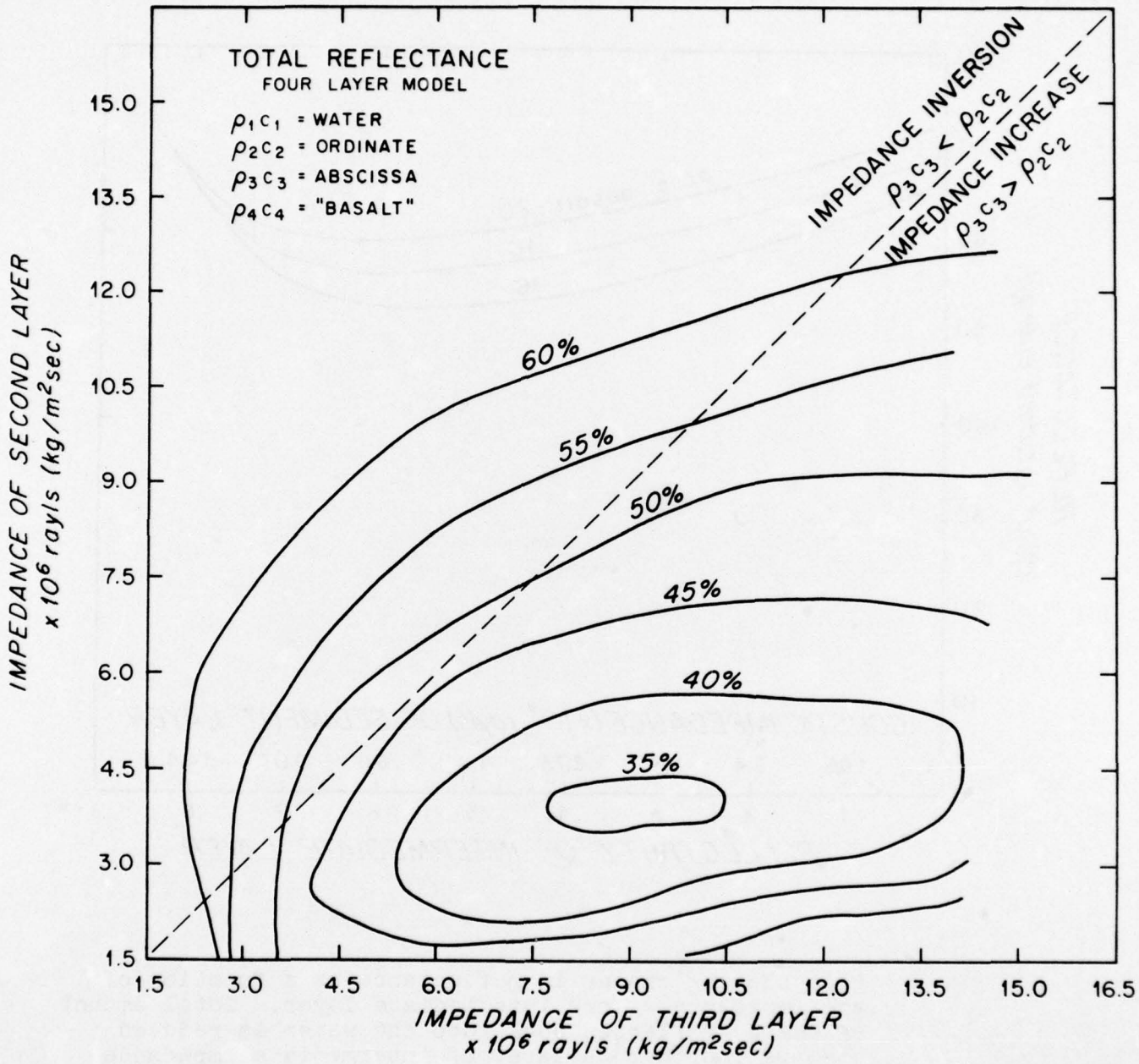

FIG. IV-3 Plot showing change in reflectance as a function of the impedance of two intermediate layers between water and basalt.

layers) the reflectance is seen to increase.

These examples in conjunction with the analysis of data that are presented illustrate ways in which an improved understanding of seismic reflection energetics can lead to refined geological interpretations of the seismic reflection profile.

Appendix V. An Estimate of the Effect of Noise on the Cumulative Energy Curves.

Two "signals" are arriving simultaneously for analysis, the desired signal is a coherent time series S(t) while the noise is a random time series N(t). For the cumulative energy curve we want the sum of the energy from the start of the signal up to a time T, or $\int_0^T (s(t))^2 dt$. Since both signal and noise are recorded, their instantaneous amplitudes add. So the signal to be processed is

$$\int_0^T \left(s(t) + N(t)\right)^2 dt = \int_0^T \left[(s(t))^2 + (N(t))^2 + 2\, s(t)\, N(t)\right] dt$$

The first term is the desired cumulative energy of the acoustic signal. The second term in the integral is the cumulative energy of the noise in the interval. We postulate that the received noise background is sufficiently uniform that we can use an average noise signal. The average noise level is computed in a 500 millisecond window before the first seafloor return, and may be designated as $\langle (N(t))^2 \rangle$. Thus the second term may be expressed as $\int_0^T (N(t))^2 dt = \langle (N(t))^2 \rangle T$. Actually in the digital processing of the data the average noise energy per digital interval is subtracted from the total energy.

The third term, $\int_0^T 2\, s(t)\, N(t)\, dt$, is more difficult to assess. It is the integral of the product of two uncorrelated time series so the instantaneous magnitude of this term is determined by the phase relations between S(t) and N(t). Both S(t) and N(t) have positive and negative values and their product may also have both positive and negative values. If this term is summed over a long time its value should be zero, however, the 50 to 100 millisecond pulse duration of the seismic source, the expected length of a reflection event, is not long enough.

The result of the digital processing of the data should thus produce the following:

$$\int_0^T (s(t) + N(t))^2 dt - \langle (N(t))^2 \rangle T = \int_0^T (s(t))^2 dt + 2\int_0^T s(t)\, N(t)\, dt$$

Obviously the lower bound of the cross-product term is zero. But zero is not its expected value in a short time interval, rather this term is indeterminable although small.

For the first seafloor arrival with a signal-to-noise ratio greater than 20 dB, the term $\int_o^\tau (s(t))^2 dt$ will be so much larger than the cross-product term that its effect is trivial. But for the second arrival with a signal-to-noise ratio near 0 dB, the magnitudes of S(t) and N(t) are nearly equal. In this case the cross-product term is very likely to be sufficiently large so that it cannot be neglected in comparison with $\int_o^\tau (s(t))^2 dt$. Thus it introduces a random error in the cumulative energy of the second arrival and also in the computation of either the sound power reflection coefficient (α) or the Rayleigh reflection coefficient (r).

MANDATORY DISTRIBUTION LIST

FOR UNCLASSIFIED TECHNICAL REPORTS, REPRINTS, & FINAL REPORTS
PUBLISHED BY OCEANOGRAPHIC CONTRACTORS
OF THE OCEAN SCIENCE AND TECHNOLOGY DIVISION
OF THE OFFICE OF NAVAL RESEARCH
(REVISED OCT. 1975)

1 Director of Defense Research and Engineering
Office of the Secretary of Defense
Washington, DC 20301
ATTN: Office Assistant Director (Research)

Office of Naval Research
Arlington, VA 22217
3 ATTN: (Code 480)
1 ATTN: (Code 460)
1 ATTN: (Code 102-OS)
6 ATTN: (Code 102IP)
1 ATTN: (Code 200)

1 LCDR David Cacchione, (USN)
ONR Representative
Woods Hole Oceanographic Inst.
Woods Hole, MA 02543

1 Office of Naval Research
Branch Office
495 Summer Street
Boston, MA 02210

Director
Naval Research Laboratory
Washington, DC 20375
6 ATTN: Library, Code 2620

1 National Oceanographic Data Center
National Oceanic & Atmospheric Administration
Rockville, MD 20852

12 Defense Documentation Center
Cameron Station
Alexandria, VA 22314

Commander
Naval Oceanographic Office
Washington, DC 20390
1 ATTN: Code 1640
1 ATTN: Code 70

Woods Hole Oceanographic Institution
WHOI-76-88

REFLECTION ENERGETICS AND ACOUSTIC IMPEDANCE OF THE SEABED FROM NORMAL-INCIDENCE SEISMIC REFLECTIONS - SOMALI BASIN by S. T. Knott, Hartley Hoskins and E. O. LaCasce, Jr. 71 pages. September 1976. Prepared for the Office of Naval Research under Contract N00014-74-C-0262; NR 083-004 and for the National Science Foundation under Grant GA-27516.

Useful estimates of seabed acoustic impedance variations in depth and location can be derived from measurements of the travel time rate at which low frequency normal incidence reflected seismic energy is received. Analysis techniques are straightforward and easily applied to station data and to traverse profiles to evaluate the lateral continuity of material properties from one location to another. Added to critical judgment, geological and geophysical evidence, e.g. drill-hole cores, outcrops and interval and critical refraction velocity measurements, reflection energetics measurements provide improved insight with which to justify classifications of seabed materials within the constraints of available information.

The analysis technique is tested using reflection data from six stations and two profiles in the environs of the Somali Basin. Two clearly different impedance-depth distributions are evident, one to the northwest of Chain Ridge is near-linear down through the sediments and including basement, the other to the south of the basin proper exhibits a near-uniform low impedance
(Cont. on back)

1. Seismic reflection profiling
2. Reflection energetics of seismic profiling
3. Acoustic impedance estimates from seismic reflections

I. Knott, S. T.
II. Hoskins, Hartley
III. LaCasce, E. O., Jr.
IV. N00014-74-C-0262; NR 083-004
V. NSF GA-27516

This card is UNCLASSIFIED

Woods Hole Oceanographic Institution
WHOI-76-88

REFLECTION ENERGETICS AND ACOUSTIC IMPEDANCE OF THE SEABED FROM NORMAL-INCIDENCE SEISMIC REFLECTIONS - SOMALI BASIN by S. T. Knott, Hartley Hoskins and E. O. LaCasce, Jr. 71 pages. September 1976. Prepared for the Office of Naval Research under Contract N00014-74-C-0262; NR 083-004 and for the National Science Foundation under Grant GA-27516.

Useful estimates of seabed acoustic impedance variations in depth and location can be derived from measurements of the travel time rate at which low frequency normal incidence reflected seismic energy is received. Analysis techniques are straightforward and easily applied to station data and to traverse profiles to evaluate the lateral continuity of material properties from one location to another. Added to critical judgment, geological and geophysical evidence, e.g. drill-hole cores, outcrops and interval and critical refraction velocity measurements, reflection energetics measurements provide improved insight with which to justify classifications of seabed materials within the constraints of available information.

The analysis technique is tested using reflection data from six stations and two profiles in the environs of the Somali Basin. Two clearly different impedance-depth distributions are evident, one to the northwest of Chain Ridge is near-linear down through the sediments and including basement, the other to the south of the basin proper exhibits a near-uniform low impedance
(Cont. on back)

1. Seismic reflection profiling
2. Reflection energetics of seismic profiling
3. Acoustic impedance estimates from seismic reflections

I. Knott, S. T.
II. Hoskins, Hartley
III. LaCasce, E. O., Jr.
IV. N00014-74-C-0262; NR 083-004
V. NSF GA-27516

This card is UNCLASSIFIED

Woods Hole Oceanographic Institution
WHOI-76-88

REFLECTION ENERGETICS AND ACOUSTIC IMPEDANCE OF THE SEABED FROM NORMAL-INCIDENCE SEISMIC REFLECTIONS - SOMALI BASIN by S. T. Knott, Hartley Hoskins and E. O. LaCasce, Jr. 71 pages. September 1976. Prepared for the Office of Naval Research under Contract N00014-74-C-0262; NR 083-004 and for the National Science Foundation under Grant GA-27516.

Useful estimates of seabed acoustic impedance variations in depth and location can be derived from measurements of the travel time rate at which low frequency normal incidence reflected seismic energy is received. Analysis techniques are straightforward and easily applied to station data and to traverse profiles to evaluate the lateral continuity of material properties from one location to another. Added to critical judgment, geological and geophysical evidence, e.g. drill-hole cores, outcrops and interval and critical refraction velocity measurements, reflection energetics measurements provide improved insight with which to justify classifications of seabed materials within the constraints of available information.

The analysis technique is tested using reflection data from six stations and two profiles in the environs of the Somali Basin. Two clearly different impedance-depth distributions are evident, one to the northwest of Chain Ridge is near-linear down through the sediments and including basement, the other to the south of the basin proper exhibits a near-uniform low impedance
(Cont. on back)

1. Seismic reflection profiling
2. Reflection energetics of seismic profiling
3. Acoustic impedance estimates from seismic reflections

I. Knott, S. T.
II. Hoskins, Hartley
III. LaCasce, E. O., Jr.
IV. N00014-74-C-0262; NR 083-004
V. NSF GA-27516

This card is UNCLASSIFIED

Woods Hole Oceanographic Institution
WHOI-76-88

REFLECTION ENERGETICS AND ACOUSTIC IMPEDANCE OF THE SEABED FROM NORMAL-INCIDENCE SEISMIC REFLECTIONS - SOMALI BASIN by S. T. Knott, Hartley Hoskins and E. O. LaCasce, Jr. 71 pages. September 1976. Prepared for the Office of Naval Research under Contract N00014-74-C-0262; NR 083-004 and for the National Science Foundation under Grant GA-27516.

Useful estimates of seabed acoustic impedance variations in depth and location can be derived from measurements of the travel time rate at which low frequency normal incidence reflected seismic energy is received. Analysis techniques are straightforward and easily applied to station data and to traverse profiles to evaluate the lateral continuity of material properties from one location to another. Added to critical judgment, geological and geophysical evidence, e.g. drill-hole cores, outcrops and interval and critical refraction velocity measurements, reflection energetics measurements provide improved insight with which to justify classifications of seabed materials within the constraints of available information.

The analysis technique is tested using reflection data from six stations and two profiles in the environs of the Somali Basin. Two clearly different impedance-depth distributions are evident, one to the northwest of Chain Ridge is near-linear down through the sediments and including basement, the other to the south of the basin proper exhibits a near-uniform low impedance
(Cont. on back)

1. Seismic reflection profiling
2. Reflection energetics of seismic profiling
3. Acoustic impedance estimates from seismic reflections

I. Knott, S. T.
II. Hoskins, Hartley
III. LaCasce, E. O., Jr.
IV. N00014-74-C-0262; NR 083-004
V. NSF GA-27516

This card is UNCLASSIFIED

throughout the sediment column with sharp increases at or near basement, in agreement with that found nearby at Deep Sea Drilling Project site #235. Continuity of material properties is more uniform in the southern data than the northern where local variations in seafloor reflectivity and seabed response are evident.

Major conclusions from our "audit" of reflected energy are that reflection energetics measurements and impedance estimates agree with and/or corroborate the other geological and geophysical evidence, and that such an audit has unique utility in the interpretation of seismic reflection profiles, particularly as to the degree of lateral continuity in the seabed physical properties. Logical extension of the technique to higher frequencies will provide higher resolution for assessing the surficial seabed characteristics.

throughout the sediment column with sharp increases at or near basement, in agreement with that found nearby at Deep Sea Drilling Project site #235. Continuity of material properties is more uniform in the southern data than the northern where local variations in seafloor reflectivity and seabed response are evident.

Major conclusions from our "audit" of reflected energy are that reflection energetics measurements and impedance estimates agree with and/or corroborate the other geological and geophysical evidence, and that such an audit has unique utility in the interpretation of seismic reflection profiles, particularly as to the degree of lateral continuity in the seabed physical properties. Logical extension of the technique to higher frequencies will provide higher resolution for assessing the surficial seabed characteristics.

throughout the sediment column with sharp increases at or near basement, in agreement with that found nearby at Deep Sea Drilling Project site #235. Continuity of material properties is more uniform in the southern data than the northern where local variations in seafloor reflectivity and seabed response are evident.

Major conclusions from our "audit" of reflected energy are that reflection energetics measurements and impedance estimates agree with and/or corroborate the other geological and geophysical evidence, and that such an audit has unique utility in the interpretation of seismic reflection profiles, particularly as to the degree of lateral continuity in the seabed physical properties. Logical extension of the technique to higher frequencies will provide higher resolution for assessing the surficial seabed characteristics.

throughout the sediment column with sharp increases at or near basement, in agreement with that found nearby at Deep Sea Drilling Project site #235. Continuity of material properties is more uniform in the southern data than the northern where local variations in seafloor reflectivity and seabed response are evident.

Major conclusions from our "audit" of reflected energy are that reflection energetics measurements and impedance estimates agree with and/or corroborate the other geological and geophysical evidence, and that such an audit has unique utility in the interpretation of seismic reflection profiles, particularly as to the degree of lateral continuity in the seabed physical properties. Logical extension of the technique to higher frequencies will provide higher resolution for assessing the surficial seabed characteristics.